ELEMENTA
Science of the Anthropocene

Amiraux, R, et al. 2019. Temporal evolution of IP_{25} and other highly branched isoprenoid lipids in sea ice and the underlying water column during an Arctic melting season. *Elem Sci Anth,* 7: 38. DOI: https://doi.org/10.1525/elementa.377

RESEARCH ARTICLE

Temporal evolution of IP_{25} and other highly branched isoprenoid lipids in sea ice and the underlying water column during an Arctic melting season

Rémi Amiraux*, Lukas Smik*, Denizcan Köseoğlu*, Jean-François Rontani†, Virginie Galindo‡, Pierre-Luc Grondin§,‖, Marcel Babin§,‖ and Simon T. Belt*

In recent years, certain mono- and di-unsaturated highly branched isoprenoid (HBI) alkene biomarkers (i.e., IP_{25} and HBI IIa) have emerged as useful proxies for sea ice in the Arctic and Antarctic, respectively. Despite the relatively large number of sea ice reconstructions based on IP_{25} and HBI IIa, considerably fewer studies have addressed HBI variability in sea ice or in the underlying water column during a spring bloom and ice melt season. In this study, we quantified IP_{25} and various other HBIs at high temporal and vertical resolution in sea ice and the underlying water column (suspended and sinking particulate organic matter) during a spring bloom/ice melt event in Baffin Bay (Canadian Arctic) as part of the Green Edge project. The IP_{25} data are largely consistent with those reported from some previous studies, but also highlight: (i) the short-term variability in its production in sea ice; (ii) the release of ice algae with high sinking rates following a switch in sea ice conditions from hyper- to hyposaline within the study period; and (iii) the occurrence of an under-ice phytoplankton bloom. Outcomes from change-point analysis conducted on chlorophyll *a* and IP_{25}, together with estimates of the percentage of ice algal organic carbon in the water column, also support some previous investigations. The co-occurrence of other di- and tri-unsaturated HBIs (including the pelagic biomarker HBI III) in sea ice are likely to have originated from the diatom *Berkeleya rutilans* and/or the *Pleurosigma* and *Rhizosolenia* genera, residing either within the sea ice matrix or on its underside. Although a possible sea ice source for HBIs such as HBI III may also impact the use of such HBIs as pelagic counterparts to IP_{25} in the phytoplankton marker-IP_{25} index, we suggest that the impact is likely to be small based on HBI distribution data.

Keywords: Spring ice melt; IP_{25}; Ice algal bloom; Under-ice algal bloom; HBIs; *Berkeleya rutilens*

1. Introduction

Highly branched isoprenoid (HBI) alkenes are unusual biomarkers made by a relatively small number of diatoms yet are common constituents in marine sediments worldwide (Robson and Rowland, 1986; Rowland and Robson, 1990; Belt et al., 2000a; Sinninghe Damsté et al., 2004). HBIs occur mainly as sester- (C_{25}) and triterpenoids (C_{30}) with between one and six double bonds (Volkman et al., 1994; Belt et al., 1996; Wraige et al., 1997; Sinninghe-Damsté et al., 1999; Belt et al., 2000a, 2001; Grossi et al., 2004), although C_{25} HBIs with one to three double bonds are the most common. In the last decade, elucidation of the sources and distributions of some HBIs has highlighted their potential as proxies for sea ice in the Polar Regions, and in a range of different sea ice settings (see Belt, 2018, 2019 for recent reviews).

The first of these HBIs, IP_{25} (ice proxy with 25 carbon atoms; Belt et al., 2007; Belt, 2018), is a mono-unsaturated C_{25} HBI (**Figure 1**), first shown to be produced by only three (or four) sympagic diatom taxa: *Pleurosigma stuxbergii* var. *rhomboides* (Cleve in Cleve & Grunow) Cleve, *Haslea kjellmanii* (Cleve) Simonsen, *H. crucigeroides* (Hustedt) Simonsen, and/or *H. spicula* (Hickie) Lange-Bertalot (Brown et al., 2014c). In a subsequent study, IP_{25} was identified in laboratory cultures of *H. spicula*, but not *H. crucigeroides* (Limoges et al., 2018), following isolation of both species from Arctic sea ice cores. In contrast, a close structural analogue of IP_{25}, but with an additional double bond in its structure (IIa; **Figure 1**), co-occurs with IP_{25} in Arctic sea ice and associated sediments

* Biogeochemistry Research Centre, School of Geography, Earth and Environmental Sciences, University of Plymouth, Drake Circus, Plymouth, Devon, UK

† Aix Marseille Univ, Université de Toulon, CNRS/INSU/IRD, Mediterranean Institute of Oceanography (MIO), Marseille, FR

‡ Institut des sciences de la mer (ISMER), Université du Québec à Rimouski, Rimouski, Québec, CA

§ Takuvik Joint International Laboratory, Laval University, CA

‖ CNRS, Département de biologie, Université Laval, Québec, CA

Corresponding author: Rémi Amiraux (remi.amiraux@plymouth.ac.uk)

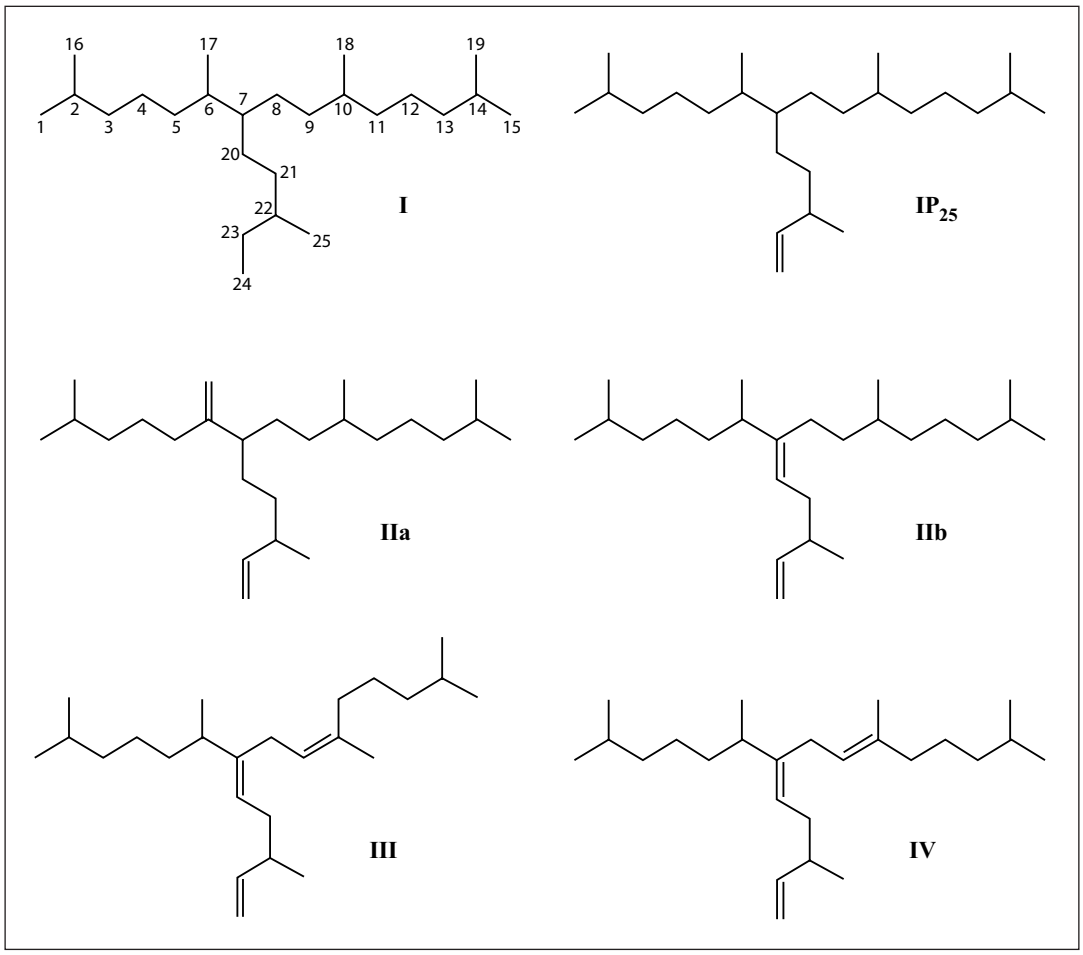

Figure 1: Structures of some common C_{25} highly branched isoprenoids (IP_{25}–IV). Numbering system used to describe structural characteristics of highly branched isoprenoids (I) and some common C_{25} highly branched isoprenoids: IP_{25}, IIa, IIb, III, and IV. DOI: https://doi.org/10.1525/elementa.377.f1

but is also present in the Antarctic. In a recent study, Belt et al. (2016) identified the Antarctic sympagic diatom *Berkeleya adeliensis* (Medlin) as a source of HBI IIa, and proposed the term $IPSO_{25}$ (ice proxy for the Southern Ocean with 25 carbon atoms) for this biomarker, at least when detected in the Antarctic (Belt et al., 2016). However, the source-specificity of HBI IIa is not as clear as that for IP_{25}, as it has also been identified in the benthic diatom *Haslea ostrearia* (Johns et al., 1999; Rowland et al., 2001b) and in sediments from some temperate locations (Xu et al., 2006; He et al., 2016). Finally, a third (at least) HBI has been identified in several *Rhizosolenia* spp. isolated from polar and sub-polar locations (Belt et al., 2017) and has been linked with open-water (pelagic) conditions in both the Arctic and the Antarctic (Massé et al., 2011; Collins et al., 2013; Belt et al., 2015, 2017; Smik et al., 2016a, 2016b; Belt, 2018). As a common constituent of marine settings (Belt et al., 2000a), this tri-unsaturated HBI, sometimes referred to as HBI III (**Figure 1**), is also showing potential as a proxy for the spring marginal ice zone (MIZ) in the Arctic and the Antarctic (Collins et al., 2013; Belt et al., 2015; Smik et al., 2016a, 2016b; Köseoğlu et al., 2018; Belt et al., 2019). The possibility of HBI III biosynthesis by other polar pelagic diatoms also needs to be considered, though previously only certain *Pleurosigma* spp. have been shown to produce this HBI, and such species are not especially common or abundant in polar environments.

Although the apparent source specificity of each HBI is of clear value from a proxy point of view, some additional information has been proposed by combining some of the respective HBI abundance characteristics in the form of various indices. For example, the phytoplankton marker-IP_{25} or PIP_{25} index (Müller et al., 2011) combines the concentration of IP_{25} with those of various pelagic biomarkers, including HBI III. In some cases, sedimentary PIP_{25} data provide more detailed descriptions of palaeo Arctic sea ice conditions than using IP_{25} alone (e.g., Fahl and Stein, 2012; Müller et al., 2012; Cabedo-Sanz, 2013; Stein and Fahl, 2013; Berben et al., 2014; Müller and Stein, 2014; Belt, 2018, 2019). A suite of pelagic biomarkers has thus far been employed in the PIP_{25} index, yet which is the most valuable in different settings or regions remains unclear. However, the use of HBI III has recently been proposed to offer some advantages over some other biomarkers, including sterols, due to its higher apparent source-specificity and closer sedimentary concentration to IP_{25}, which removes, to some extent, the problems of the c-factor used in the PIP_{25} calculation (see Smik et al., 2016b, for more detailed discussions of this topic). In a different application, IP_{25} concentrations have been combined with particulate organic carbon data from sea ice

and the underlying water column to estimate the proportion of sea ice algal-derived organic carbon within a mixed pool during the period of sea ice melting in spring (Brown et al., 2016).

Despite the growing use of IP_{25} and other HBIs for palaeo sea ice reconstruction and polar food web studies (e.g., Brown et al., 2017, 2018; Belt, 2018), the number of studies aimed at measuring these lipids in sea ice and in the underlying water column along the ice-covered season remains relatively limited (see Belt, 2018, for a summary). Further, such studies were focused mainly on one or two HBIs or a single environmental component (e.g., sea ice, suspended, sinking or sediment POM; Brown et al., 2011; Belt et al., 2013; Rontani et al., 2014), were conducted at relatively low temporal or vertical resolution (Belt et al., 2013; Brown et al., 2016, 2017), combined data from different locations (Brown and Belt, 2012; Fahl and Stein, 2012) or were conducted in somewhat niched oceanic settings, including fjords (Limoges et al., 2018). In this study, we obtained a high-resolution temporal and vertical (multiple sample type and depth) dataset of HBI concentrations across an entire melting season in the Arctic, as part of the Green Edge project, in order to provide a more integrated dataset for building on previous investigations and gain further insights into the use of HBIs as Arctic sea ice proxies.

2. Materials and Methods

2.1. Sampling

The sampling was conducted at a landfast station near Broughton Island (67°28.766'N; 63°47.579'W; water column depth of 350 m; **Figure 2**) in Baffin Bay (Canadian

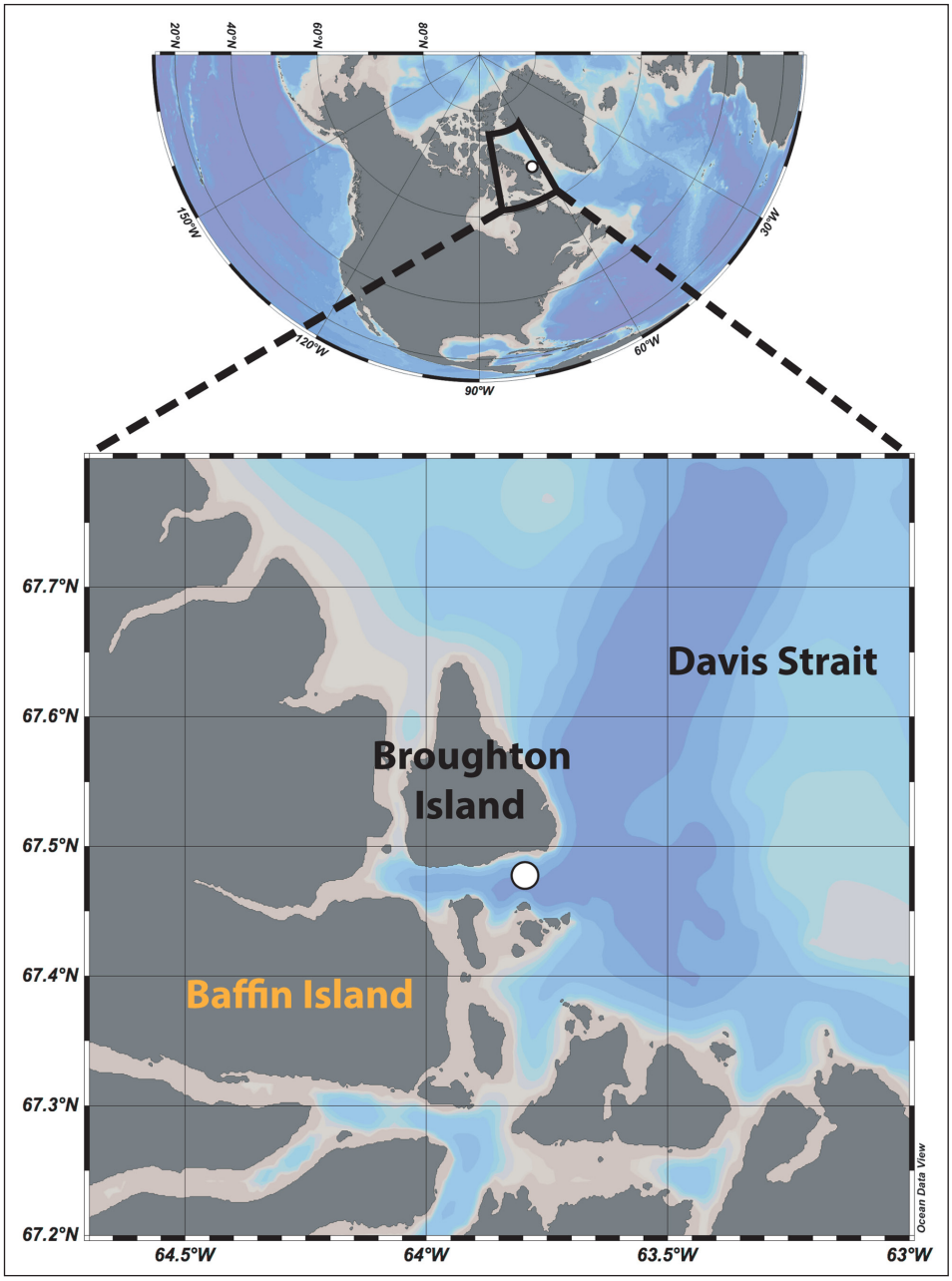

Figure 2: Map of the study area with location of the station investigated in Baffin Bay. White circle on the enlarged map of western Baffin Bay indicates the sampling location. DOI: https://doi.org/10.1525/elementa.377.f2

Arctic) from 16 May to 8 July 2016 within the framework of the Green Edge project. This study location was selected because of (i) the presence of seasonal sea ice; (ii) the recurrence of ice edge blooms in July that follow the seasonal ice breakup which, in 2016, occurred on 21 July (Oziel et al., 2019); and (iii) the presumed representation of a suitable model for the whole Arctic Ocean in terms of physical and biological processes (for a review, see Oziel et al., 2019).

2.1.1. Sea ice

Two sets of sea ice sampling were carried out, with both using a Kovacs Mark V 14-cm diameter corer and focusing on the bottom-most 10 cm of sea ice where the majority of ice biota are found (Smith et al., 1990). The first set of samples were sub-sectioned into two further intervals (0–3 and 3–10 cm) and are referred to hereafter as the low vertical resolution (LVR) samples. The second set of samples were further divided into five sub-sections (0–1, 1–2, 2–5, 5–7, and 7–10 cm) and represent the high vertical resolution (HVR) series. The LVR sampling set was collected every 2–3 days, while the HVR sampling set was collected on 17 sampling dates over the study period. To compensate for biomass heterogeneity, common in sea ice (Gosselin et al., 1986), three or four equivalent core sections were pooled for each sampling day in isothermal containers. Pooled sea ice sections were then melted in the dark with 0.2-μm filtered seawater (FSW; 3:1 v:v) to minimize osmotic stress on the microbial community during melting (Bates and Cota, 1986; Garrison and Buck, 1986). Two additional entire sea ice cores were collected to measure the sea ice temperature and salinity, thus allowing the calculation of brine salinity and volume (Cox and Weeks, 1983). Sea ice internal core temperatures were measured using a Testo 720 temperature probe inserted into a hole drilled to the centre of the core every 10 cm, while salinity was measured in melted (10-cm) sea ice sections using a conductivity meter (Orion portable salinometer model WP-84TPS, Thermo Scientific) calibrated against 15 N KCL solution at 20°C.

2.1.2. Water column

Suspended particulate matter (SPM) was collected on 16 sampling dates over the study period at depths of 1.5, 10, 20 and 40 m (60 m, not 40 m, for the last five sampling dates) under the sea ice using large (20 L) Niskin bottles to accommodate any within-sample heterogeneity. SPM was also collected at the ice/water interface, using a battery-operated plastic submersible pump (Cyclone®) secured to the end of an articulated under-ice arm through an ice auger-drilled hole. Vertical profiles of salinity in the water column were measured using a Sea-Bird SBE 19plus V2 conductivity-temperature-depth (CTD) probe on all sampling days. Photosynthetically active radiation (PAR) was estimated using the multispectral data collected with a Compact – Optical Profiling System (C-OPS; version Ice-PRO; Biospherical instruments Inc.) (see Oziel et al., 2019).

Short-term sediments traps were deployed at 2 and 25 m with two mooring lines at the same geographical coordinates as the SPM and sea ice samples. Sediment traps were immersed for approximately 48 h and were recovered at the same frequency as for the LVR sea ice sampling. Sediment traps were made of polyvinyl chloride (PVC) and had an aperture diameter of 15 cm.

Samples of each sample type were filtered through pre-weighed Whatman glass fibre filters (porosity 0.7 μm, diameter 25 or 47 mm, pre-combusted 4 h at 450°C) and kept frozen (<–20°C) prior to lipid analysis.

2.2. Analysis of HBI biomarkers

Extraction of HBI lipids was carried out according to methods described previously (Belt et al., 2012). To enable quantification, an internal standard (9-octyl-8-hepta-decene; 0.02 μg) was added to each filter prior to extraction. Filters were then saponified (10% KOH; 90°C, 120 min; 10 mL), after which the non-polar fraction containing HBI lipids was collected using open column silica chromatography (ca. 1 g silica; 6–7 mL hexane; Belt et al., 2012). Analysis of HBIs was carried out using gas chromatography–mass spectrometry (GC–MS) in selected ion monitoring (SIM, *m/z* 350 for IP_{25}, 348 for HBIs IIa and IIb, and 346 for HBIs III and IV) mode using an Agilent 7890 series gas chromatograph (HP_{5MS} fused silica column; 30 m × 0.25 mm i.d., 0.25-μm film thickness) coupled to an Agilent 5975 mass spectrometric detector (Belt et al., 2012). HBIs were identified by comparison of retention indices and mass spectra to those of authentic standards (Belt et al., 2000a; Belt, 2018). HBIs (pg mL^{-1}) were quantified by comparing mass spectral intensities of molecular ions to that of the internal standard, and normalizing for differences in mass spectral fragmentation efficiency and volume filtered (ca. 30–1000, 900, 40–80 mL for sea ice, suspended and sinking particles, respectively).

2.3. Algal biomass

At the shore-site laboratory, and within 24 h of sampling, duplicate samples of sea ice, suspended and sinking POM were filtered through Whatman GF/F glass fibre filters. Concentration of chlorophyll *a* (Chl *a*) retained on the filters was measured using a TD-700 Turner Designs fluorometer, after 18–24 h extraction in 90% acetone at –20°C in the dark (Parsons et al., 1984). The fluorometer was calibrated with a commercially available Chl *a* standard (*Anacystis nidulans*, Sigma).

2.4. Protist assemblage

The protist assemblage was determined using an Imaging FlowCytobot (IFCB, Woods Hole Oceanographic Institute). For each melted ice and seawater samples, 5 mL were analyzed. A 150-μm Nitex mesh was used to avoid blocking of the fluidics system by large particles, although this step might have introduced a bias in the results by preventing the sampling of large cells. Images were processed using a custom made MATLAB (R2013b) code (Sosik and Olson, 2007; processing codes are available at https://github.com/hsosik/ifcb-analysis). Automatic classification was performed using random forest algorithms with the EcoTaxa application (Picheral et al., 2015). A learning set was manually prepared with ca. 20,000 images annotated and used for automatic prediction. Images were classified

into 35 categories. Each automatically annotated image was further validated by visual examination and corrected when necessary.

2.5. Ice-derived particulate organic carbon in seawater (%iPOC$_w$)

As the contribution of particulate inorganic carbon (PIC) to total particulate carbon (TPC) is considered negligible in the ocean (<6%; Gordon, 1971; Gardner et al., 2003), we used values of TPC as a surrogate for particulate organic carbon (POC) to enable us to estimate values of %iPOC$_w$ according to the method of Brown et al. (2016). Briefly, estimates of iPOC$_w$ in individual seawater samples were obtained by multiplying IP_{25} concentrations measured in seawater (IP_{25w}) with the ratio of ice-derived POC and IP_{25} in sea ice (Equation 1) obtained from the 0–3 cm sea ice section taken on 17 June, the date of the highest IP_{25} concentration.

$$iPOC_w = IP_{25w} \times (iPOC_i / IP_{25i}) \quad \text{(Equation 1)}$$

Percentage concentration estimates of iPOC$_w$ were calculated using Equation 2, where tPOC$_w$ is the total POC measured in seawater:

$$\%iPOC_w = 100 \times (iPOC_w / tPOC_w) \quad \text{(Equation 2)}$$

2.6. TPC analyses

At the shore-site laboratory, duplicate samples of sea ice and suspended POM were filtered through pre-weighed GF/F filters (pre-combusted 24 h at 450°C) and stored prior to dry weight and TPC analysis. At Université Laval, filters were dried for 24 h at 60°C, weighed again for dry weight determination, and then analyzed using a Perkin Elmer carbon-hydrogen–nitrogen–sulfur (CHNS) 2400 Series II to measure TPC. Instrument calibration was achieved using accurately weighed samples of acetanilide (C_8H_9NO).

2.7. Statistical analyses

Correlation change-point analyses (Cabrieto et al., 2017; Cabrieto et al., 2018) were carried out using a cp3o (change points via probabilistically pruned objective; James and Matteson, 2015) test to identify the approximate timing of significant correlation shifts between variables in SPM samples along the sampling interval. Pearson's correlation with a sampling window of 11 was run using the product-moment correlation coefficient (r), as a measure of association between variables and correlation significance determined at $p \leq 0.05$. Statistical tests were carried out using R v.3.5 software (R development Core team 2018).

3. Results

3.1. Sea ice

During the period investigated, snow and ice thicknesses decreased from 32.0 to 1.8 cm and from 128 to 105 cm, respectively (**Figure 3A**). A particularly noticeable decrease can be seen for snow and ice thickness from 3 June and 17 June, respectively. Brine salinity (calculated using the whole sea ice core) also decreased during the study period from 50.5 to 17.2, while brine volume percentage (relative to sea ice) increased from ca. 6% to ca. 15% (**Figure 3B**). A switch from hyper- to hypo-saline conditions (relative to seawater) in brines took place around 6 June. Moreover, the relative brine volume in the bottom 10 cm of sea ice cores was always greater than 5% throughout the sampling period. Some potential sources of IP_{25}, HBI IIa and HBI III (e.g., *Haslea* spp., *Rhizosolenia* spp. and *Pleurosigma* spp.) were identified in some of the ice samples, although identification to only the genus level prevented definitive assignments from being made. The concentrations of Chl *a* and IP_{25} in the bottom 0–3 cm of sea ice were quantifiable for the majority of the sampling dates, with values ranging from 0.9 to 317.3 μg L^{-1} (mean ± SD = 119.8 ± 87.0 μg L^{-1}; n = 24) and 0 to 1071.1 pg mL^{-1} (mean ± SD = 239.8 ± 255.2 pg mL^{-1}; n = 48) (**Figure 3C**), respectively. Lowest concentrations for both Chl *a* and IP_{25} were observed at the first and last three sampling dates (below 43.3 μg L^{-1} and 16.0 pg L^{-1}, respectively), while their maxima were observed on 1 June and 17 June (317.3 μg L^{-1} and 1071.1 pg L^{-1} for Chl *a* and IP_{25}, respectively). With the exception of the first and last two sampling dates, IP_{25} concentration in the lower 0–3 cm section was always higher than that in the 3–10 cm section, with a mean enhancement factor in the lower section of 10.7 (**Table 1**; n = 84). However, this enhancement factor was 18.0 from 16 May to 6 June, and 7.0 from 8 June to 4 July (n = 40 and 56, respectively).

The overall trend in IP_{25} concentration between the LVR and HVR sea ice sample sets were similar, with highest values observed on 17 June and the lowest at the beginning and end of sampling (**Tables 1, 2**). Analysis of vertical IP_{25} content in the HVR sampling set (**Table 2**) revealed similar outcomes to those described above for the LVR samples, but with more subtle changes in the IP_{25} distribution due to the increased resolution. Thus, in the early part of sampling (18 May to 8 June) IP_{25} content was predominantly in the 0–2 cm sections (>86%). From ca. 8 June to 27 June, although highest IP_{25} concentrations were also found in the 0–2 cm sections, an increasing % characterized the upper layers (i.e., 2–10 cm). Finally, from 27 June to the end of sampling, IP_{25} was largely absent, with only trace amounts detected in the 1–2 cm section on 1 July (**Table 2**).

HBI IIa was also present in the majority of the samples where IP_{25} could be identified, and the two biomarkers were strongly correlated (r = 0.87, **Table 3**). Three other HBIs could also be identified, but only in the first half of the sampling period. Thus, HBIs IIb, III, and IV could be quantified in the bottom 10 cm of the two sets of sea ice samples from 16 May to 6 June with strong correlations between them (**Tables 3, 4**). In contrast, neither IP_{25} nor HBI IIa correlated with HBIs IIb, III or IV. Overall, the concentrations of all HBIs were normally higher in the 0–1 cm bottom sections, with the exception of 1 July (**Table 2**).

3.2. Suspended POM

The under-ice seawater exhibited relatively consistent hydrographic conditions from the surface (i.e., the sea ice/seawater interface) to 40 m from the beginning of

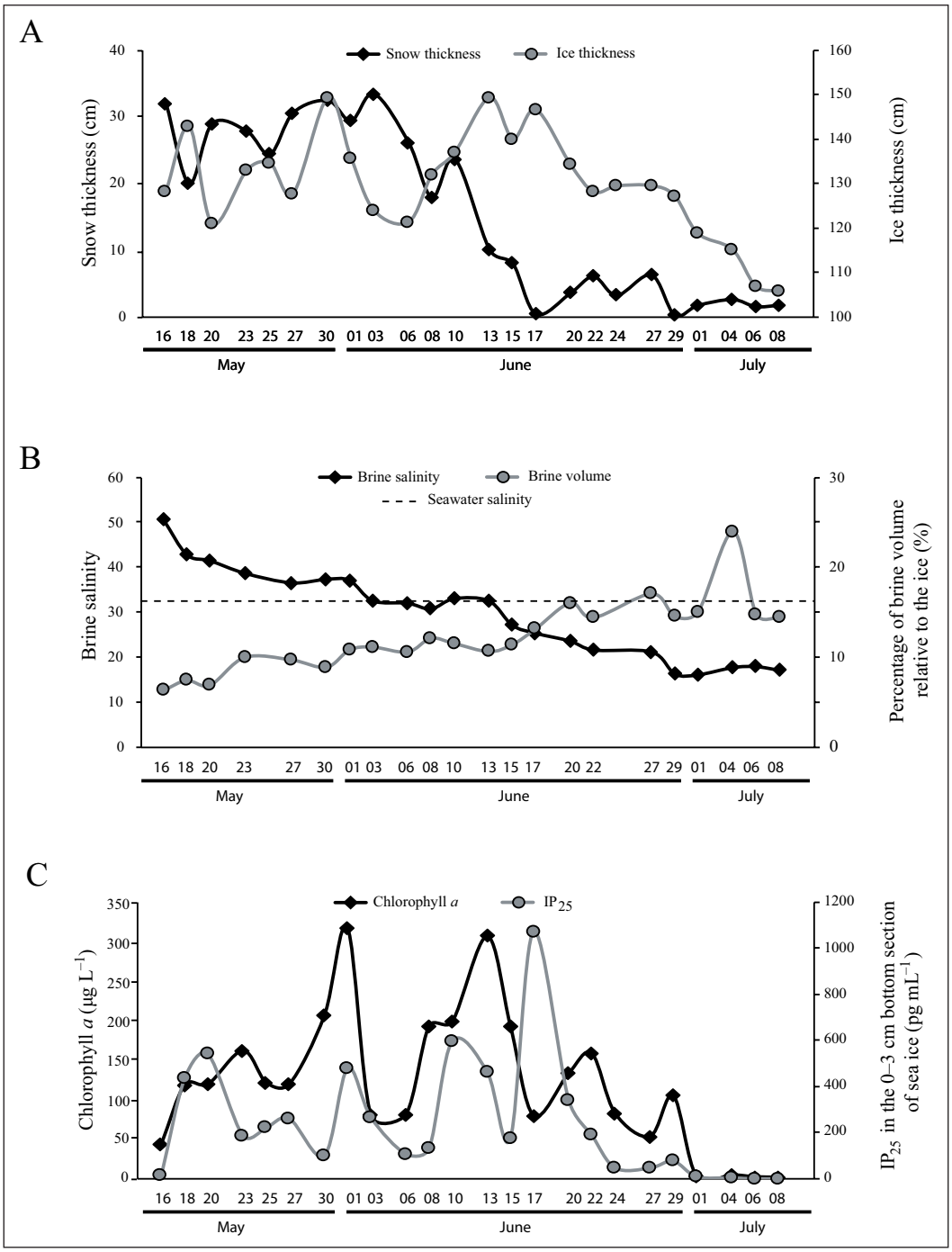

Figure 3: Time series of core parameters and biomarkers in sea ice. Time series of **(A)** snow and ice thickness, **(B)** brine salinity and brine volume, calculated from the whole sea ice core, and **(C)** Chl *a* and IP_{25} concentration in the bottom 0–3 cm sea ice section from 16 May to 8 July 2016 at the sampling location in Baffin Bay (Figure 2). DOI: https://doi.org/10.1525/elementa.377.f3

sampling to 10 June. The temperature was always in the range of −1.7 to −1.65°C and the salinity from 32.5 to 32. After 10 June, the near-surface temperature began to increase (up to −1.3°C) along with a decrease in salinity (<30; **Figure 4A, B**), which coincided with reducing sea ice thickness (**Figure 3A**). By 8 July, these trends were also evident at 10 m (i.e., −1.45°C and 32 salinity, respectively). In the early part of sampling, PAR was extremely low (mean < 0.08 mol photons m^{-2} d^{-1}; n = 2159) in the under-ice seawater until 3 June (**Figure 4C**), after which, it increased rapidly and also extended to detectable levels at 30 m by 17 June. This increase coincided with the steep decrease in snow thickness from 33.4 to 0.4 cm between 3 June and 17 June. By 8 July, PAR had increased in the near-surface waters to ca. 10 mol photons m^{-2} d^{-1}, and all isolumes were shallower.

Chl *a* concentration in the first 40 m of the water column was relatively low until 24 June, when it increased rapidly to reach 6 µg L^{-1} between 10 and 30 m by 8 July (**Figure 4D**). Near-surface Chl *a* (surface and/or 1.5 m) exhibited three anomalies with relatively high or low concentration compared to surrounding waters.

Table 1: Mean IP_{25} concentration in sea ice (low vertical resolution), suspended and sinking POM during the sampling period investigated. DOI: https://doi.org/10.1525/elementa.377.t1

Sample type (units for IP_{25} content)	Sample depth	Sampling date (day/month)																						
		16/5	18/5	20/5	23/5	25/5	27/5	30/5	1/6	3/6	6/6	8/6	10/6	13/6	15/6	17/6	20/6	22/6	24/6	27/6	29/6	1/7	4/7	6/7	8/7
Sea ice POM (pg mL^{-1})	3–10 cm[a]	23.9	24.2	24.2	17.5	19.0	3.7	7.9	50.6	21.9	8.1	22.2	65.0	117.1	41.8	238.2	12.4	24.8	10.8	18.6	20.3	4.6	4.3	2.2	7.6
	0–3 cm[b]	16.0	434.4	539.4	186.9	220.3	259.9	99.6	477.9	265.8	107.1	130.5	595.7	462.5	176.2	1071.1	341.8	188.5	46.8	45.9	75.8	4.4	3.4	nd[c]	nd
Suspended POM (pg mL^{-1})[d]	Interface	–[e]	0.4	0.3	0.7	0.2	–	–	–	–	3.8	–	0.5	1.8	–	1.5	1.2	–	13.2	0.6	0.7	0.6	1.0	0.5	0.5
	1.5 m	–	nd	nd	nd	nd	–	–	–	–	3.6	–	0.2	0.4	–	0.5	0.5	–	0.7	0.4	0.8	nd	0.3	nd	nd
	10 m	–	nd	nd	nd	nd	–	–	–	–	0.6	–	0.4	0.8	–	1.0	0.7	–	0.9	0.7	0.9	nd	0.8	nd	0.5
	20 m	–	nd	nd	nd	nd	–	–	–	–	0.7	–	0.3	0.9	–	0.9	0.7	–	0.8	0.4	0.6	0.5	0.5	0.2	nd
	40/60 m	–	nd	nd	nd	nd	–	–	–	–	0.3	–	0.6	0.3	–	0.5	0.3	–	0.7	0.1	nd	nd	0.2	nd	nd
Sinking POM (ng m^{-2} d^{-1})	2 m[f]	–	–	–	–	–	nd	nd	nd	nd	123.4	nd	17.1	32.5	247.9	599.1	158.4	98.3	–	55.8	195.7	60.9	69.7	–	51.0
	25 m[g]	–	–	–	–	–	15.0	17.4	26.8	nd	12.8	58.1	33.3	67.8	409.8	384.5	271.8	336.9	–	200.1	207.2	92.0	166.0	–	103.9

[a] Mean relative standard deviation (SD) for duplicate samples: 32.5%, n = 48.
[b] Bottom of ice core; mean relative SD for duplicate samples: 15.4%, n = 48.
[c] Not detected.
[d] Mean relative SD for duplicate samples: 17.3%, n = 160.
[e] Not measured.
[f] Mean relative SD for duplicate samples: 13.3%, n = 34.
[g] Mean relative SD for dupliciate samples: 10.8%, n = 34.

Table 2: IP_{25} concentration (pg mL^{-1}) in sea ice POM (high vertical resolution) during the sampling period investigated. DOI: https://doi.org/10.1525/elementa.377.t2

Sea ice section	Sampling date (day/month)															
	18/5	20/5	23/5	25/5	27/5	30/5	6/6	8/6	13/6	17/6	20/6	22/6	24/6	27/6	1/7	4/7	8/7
7–10 cm	3.6	1.7	1.4	67.8	2.5	15.5	5.2	6.2	8.1	28.2	9.0	7.1	0.9	1.5	nd[a]	nd	nd
5–7 cm	5.0	1.2	2.9	8.9	4.0	10.5	7.8	7.8	28.5	64.6	14.4	13.2	2.0	2.8	nd	nd	nd
2–5 cm	9.6	3.0	5.0	15.4	5.2	37.7	20.1	15.2	70.1	151.8	29.6	27.6	2.2	5.5	nd	nd	nd
1–2 cm	39.9	15.4	5.9	38.7	14.1	67.9	57.3	46.6	197.3	153.1	40.7	22.9	nd	5.4	4.0	nd	nd
0–1 cm[b]	179.4	417.4	212.0	241.4	300.9	394.7	426.5	128.5	439.0	433.9	202.4	117.7	15.3	8.8	nd	nd	nd

[a] Not detected.
[b] Bottom of ice core.

Table 3: Correlation coefficients between biomarkers in sea ice, suspended and sinking POM. DOI: https://doi.org/10.1525/elementa.377.t3

Sample type	Factor	Chlorophyll *a*	IP_{25}	HBI IIa	HBI IIb	HBI III
Sea ice POM	Chlorophyll α	1.00	–[b]	–	–	–
	IP_{25}	0.60*[a]	1.00	–	–	–
	HBI IIa	0.79*	0.87*	1.00	–	–
	HBI IIb	n/a[c]	0.45*	0.48*	1.00	–
	HBI III	0.40*	0.44*	0.50*	0.93*	1.00
	HBI IV	0.36*	0.43*	0.48*	0.93*	0.90*
Suspended POM	Chlorophyll α	1.00	–	–	–	–
	IP_{25}	0.16	1.00	–	–	–
	HBI IIa	0.16*	n/a	1.00	–	–
	HBI IIb	n/a	n/a	n/a	1.00	–
	HBI III	n/a	n/a	n/a	n/a	1.00
	HBI IV	n/a	n/a	n/a	n/a	n/a
Sinking POM	Chlorophyll α	1.00	–	–	–	–
	IP_{25}	0.18	1.00	–	–	–
	HBI IIa	0.10	0.95*	1.00	–	–
	HBI IIb	n/a	0.49*	0.27*	1.00	–
	HBI III	0.12	0.57*	0.41*	0.77*	1.00
	HBI IV	–0.063	0.64*	0.47*	0.86*	0.80*

[a] Asterisk indicates significant correlation: $p < 0.05$.
[b] Repetition of value.
[c] Not applicable.

Relatively high values were observed from 3 June to 6 June as well as on 24 June (**Figure 4D**), which is also the case for IP_{25} (**Table 1**). Both events coincided with relatively low sea ice Chl *a* and IP_{25} content (**Figure 3C**), with the first event also occurring as brine salinity switched to hyposaline (**Figure 3B**). On the other hand, the occurrence of relatively low Chl *a* concentration in near-surface waters on 8 July coincided with low IP_{25} concentration. During both instances of higher Chl *a* concentration in near-surface waters, the protist community composition resembled that of the sea ice. In contrast, the protist composition at the time of the relatively low Chl *a* event was more similar to that of the 20 m (or deeper) waters (**Figure 5**), with a shift from pennate to centric diatoms, and most notably to *Chaetoceros* spp. As with the sea ice samples, some possible sources of IP_{25}, HBI IIa and HBI III (e.g., *Haslea* spp., *Rhizosolenia* and *Pleurosigma* spp.) were identified in some of the water samples, though only to the genus level. IP_{25} was detectable in the surface waters (i.e., the sea ice/seawater interface) throughout the sampling campaign with higher concentration from 6 June to 8 July compared to 16 May to 3 June (mean ± SD = 2.2 ± 3.6 and 0.4 ± 0.2 pg mL^{-1} respectively; n = 24 and 8, respectively; **Table 1**). Furthermore, IP_{25} concentration in surface waters was substantially higher compared to the deeper samples. Indeed, its presence below 40 m was only detected from 6 June (**Table 1**), with a mean concentration thereafter 6.7 times lower than at the surface.

Estimates for $\%iPOC_w$ ranged from 0 to 193.9% and were further normalized to a maximum of 100% for illustration purposes only (**Figure 6**). The $\%iPOC_w$ estimates for surface waters followed the same trend as IP_{25}, with relatively high values from 3 June to 6 June and again on 24 June (100 and 80.5 %, respectively). Estimates for $\%iPOC_w$ were also higher in surface water samples compared to their deeper counterparts throughout sampling (**Figure 6**). According to our $\%iPOC_w$ estimates, although ice algal contribution was relatively low in the water column (apart from surface waters) at the beginning and end of sampling (mean $\%iPOC_w$ ± SD = 1.2 ± 2.2% from 16 to 25 May and from 27 June to 8 July; n = 40 and 120, respectively), somewhat higher values were observed from 3 June to 24 June (mean $\%iPOC_w$ ± SD = 17.2 ± 10.2%; n = 60).

A decrease in the correlation between IP_{25} and Chl *a* was observed between sea ice and suspended POM (r of 0.6 and 0.16, respectively). Importantly, correlation change-point analysis between Chl *a* and IP_{25} in suspended POM showed a reduction in correlation for the shallow sample depths (i.e., the interface and 1.5-m depth) at a later date (27 June) compared to the deeper ones (i.e., at 10, 20 and 40 m; 13 June) (**Figure 7A, B**).

IP_{25} and HBI IIa concentrations in suspended particles were well correlated, as previously observed in sea ice (**Table 3**), but correlations between HBIs IIb, III and IV were difficult to assess, reliably, due to the small sample

Table 4: Mean HBI III concentration in sea ice (low vertical resolution), suspended and sinking POM during the sampling period investigated. DOI: https://doi.org/10.1525/elementa.377.t4

Sample type (units for HBI III content)	Sample depth	Sampling date (day/month)																							
		16/5	18/5	20/5	23/5	25/5	27/5	30/5	1/6	3/6	6/6	8/6	10/6	13/6	15/6	17/6	20/6	22/6	24/6	27/6	29/6	1/7	4/7	6/7	8/7
Sea ice POM ($pg\ mL^{-1}$)	3–10 cm[a]	nd[b]	nd	1.4	nd	0.6	nd	0.7	nd	1.7	0.4	nd	1.5	nd	nd	nd	nd	nd	nd	nd	nd	nd	nd	nd	nd
	0–3 cm[c]	nd	66.3	34.8	14.9	7.4	24.1	12.4	16.4	18.8	2.6	0.3	30.1	nd	nd	nd	nd	nd	nd	0.4	nd	nd	nd	nd	nd
Suspended POM ($pg\ mL^{-1}$)[d]	Interface	–[e]	nd	nd	nd	nd	–	–	–	–	0.3	–	nd	nd	–	nd	nd	–	nd	nd	nd	nd	nd	nd	nd
	1.5 m	–	nd	nd	nd	nd	–	–	–	–	0.1	–	nd	nd	–	nd	nd	–	nd	nd	nd	nd	nd	nd	nd
	10 m	–	nd	nd	nd	nd	–	–	–	–	0.1	–	nd	nd	–	nd	nd	–	nd	nd	nd	nd	nd	nd	nd
	20 m	–	nd	nd	nd	nd	–	–	–	–	0.2	–	nd	nd	–	nd	nd	–	nd	nd	nd	nd	nd	nd	nd
	40/60 m	–	nd	nd	nd	nd	–	–	–	–	nd	–	nd	nd	–	nd	nd	–	nd	nd	nd	nd	nd	nd	nd
Sinking POM ($ng\ m^{-2}\ d^{-1}$)	2 m[f]	–	–	–	–	–	nd	nd	nd	nd	3.2	nd	1.7	nd	12.4	4.1	nd	nd	–	nd	nd	nd	nd	–	nd
	25 m[g]	–	–	–	–	–	nd	1.7	nd	nd	nd	nd	1.8	2.7	2.8	8.7	nd	nd	–	2.5	6.4	nd	4.2	–	nd

[a] Mean relative standard deviation (SD) for duplicate samples: 11.5%, n = 48.
[b] Not detected.
[c] Bottom of ice core; mean relative SD for duplicate samples: 5.1%, n = 48.
[d] Mean relative SD for duplicate samples: 2.6%, n = 160.
[e] Not measured.
[f] Mean relative SD for duplicate samples: 8.8%, n = 34.
[g] Mean relative SD for duplicate samples: 24.0%, n = 34.

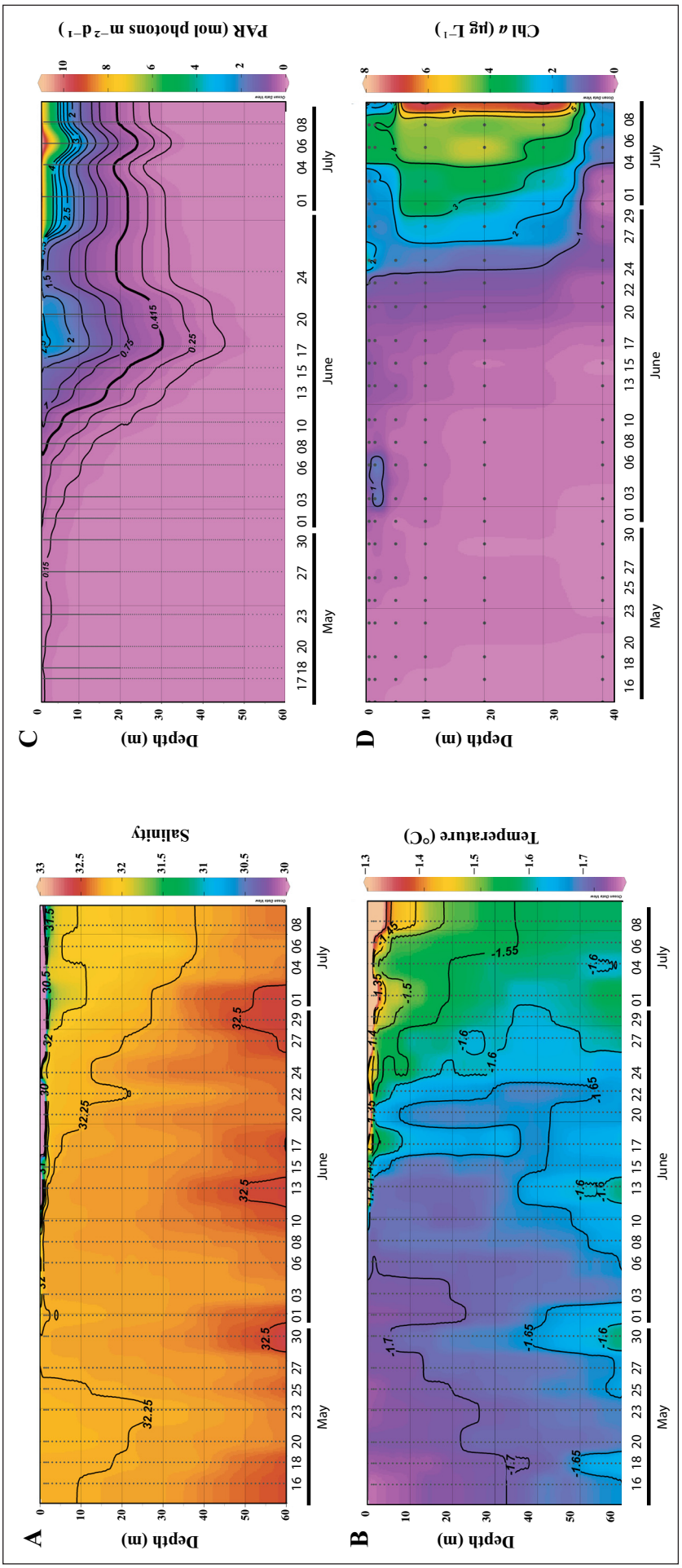

Figure 4: Time series of core parameters and biomarkers in seawater. Time series of water column **(A)** salinity, **(B)** temperature, **(C)** PAR and **(D)** Chl *a* from 16 May to 8 July 2016 at the sampling location in Baffin Bay (Figure 2). Data were interpolated and plotted using Ocean Data View v4.7.8 (Schlitzer, 2016). DOI: https://doi.org/10.1525/elementa.377.f4

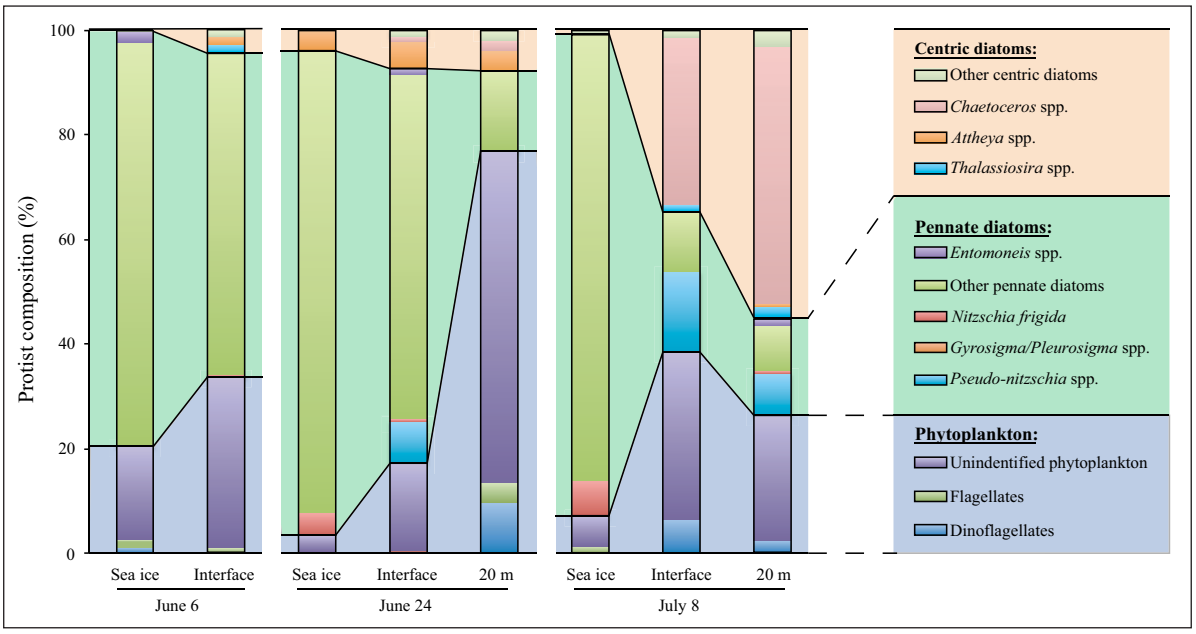

Figure 5: Relative abundance of protists in sea ice and seawater. Relative abundance of centric diatoms, pennate diatoms and phytoplankton (unidentified, flagellates and dinoflagellates) in the bottom 3 cm of sea ice and in seawater at the ice/water interface on 6 June, 24 June and 8 July and from 20-m depth on 24 June and 8 July 2016 at the sampling location in Baffin Bay (Figure 2). DOI: https://doi.org/10.1525/elementa.377.f5

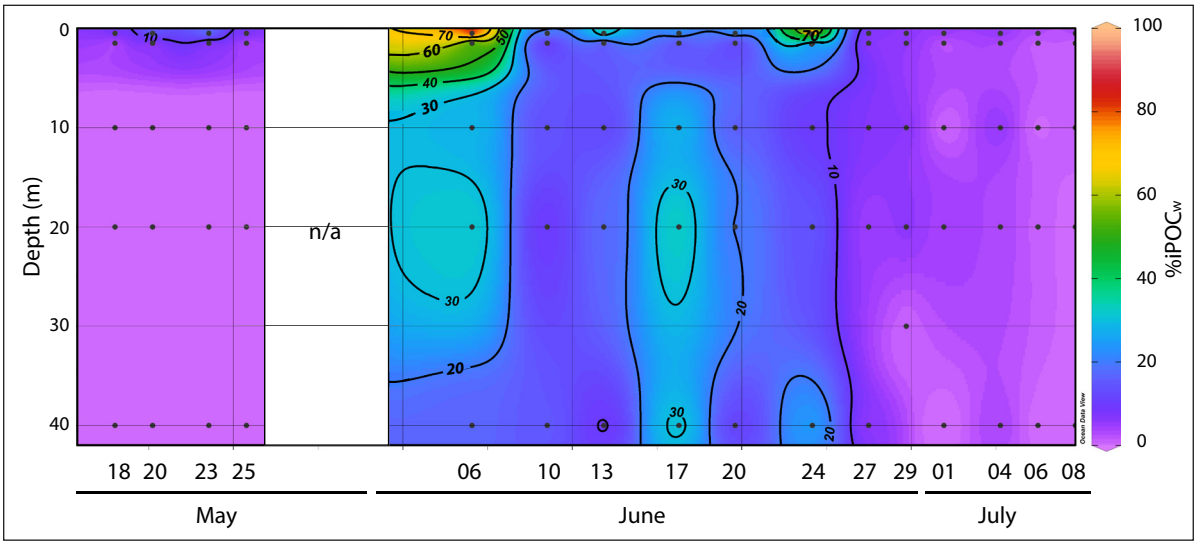

Figure 6: Time series of ice-derived POC (%iPOC$_w$) in seawater. Time series of water column iPOC$_w$ as a proportion of total organic carbon (%iPOC$_w$) from 18 May to 8 July 216 at the sampling location in Baffin Bay (Figure 2). Data were interpolated and plotted using Ocean Data View v4.7.8 (Schlitzer, 2016). Data were not available (n/a) for interpolation between 25 May and 6 June. DOI: https://doi.org/10.1525/elementa.377.f6

numbers where they could be quantified accurately. For samples where each of HBIs IIb, III and IV were quantifiable, concentrations of HBI III were, on average, 1.6 and 4.6 times lower than those of HBI IIb and IV, respectively.

Highest concentrations of HBIs III and IV in seawater were observed for the surface sample on 6 June (**Table 4**), which also coincided with the second highest IP_{25} value (**Table 1**). HBI IV was mostly detected at the surface between 16 May and 17 June, while HBI III was only detected on 6 June.

3.3. Sinking POM

IP_{25} concentration in sinking POM ranged from 0 to 599.1 ng m^{-2} d^{-1} (mean ± SD = 56.9 ± 13.9 ng m^{-2} d^{-1}; n = 34) and from 0 to 409.8 ng m^{-2} d^{-1} (mean ± SD = 73.4 ± 9.9 ng m^{-2} d^{-1}; n = 34) at 2 and 25 m, respectively. Although IP_{25} was detectable in each of the 25-m sediment trap samples, it was not identified in the 2-m trap between 16 May and 6 June (**Table 1**). Further, IP_{25} content was generally higher in the 25-m sediment trap samples compared with those at 2 m. Exceptions were found on 6 June and 17 June, dates that also coincided with relatively high IP_{25}

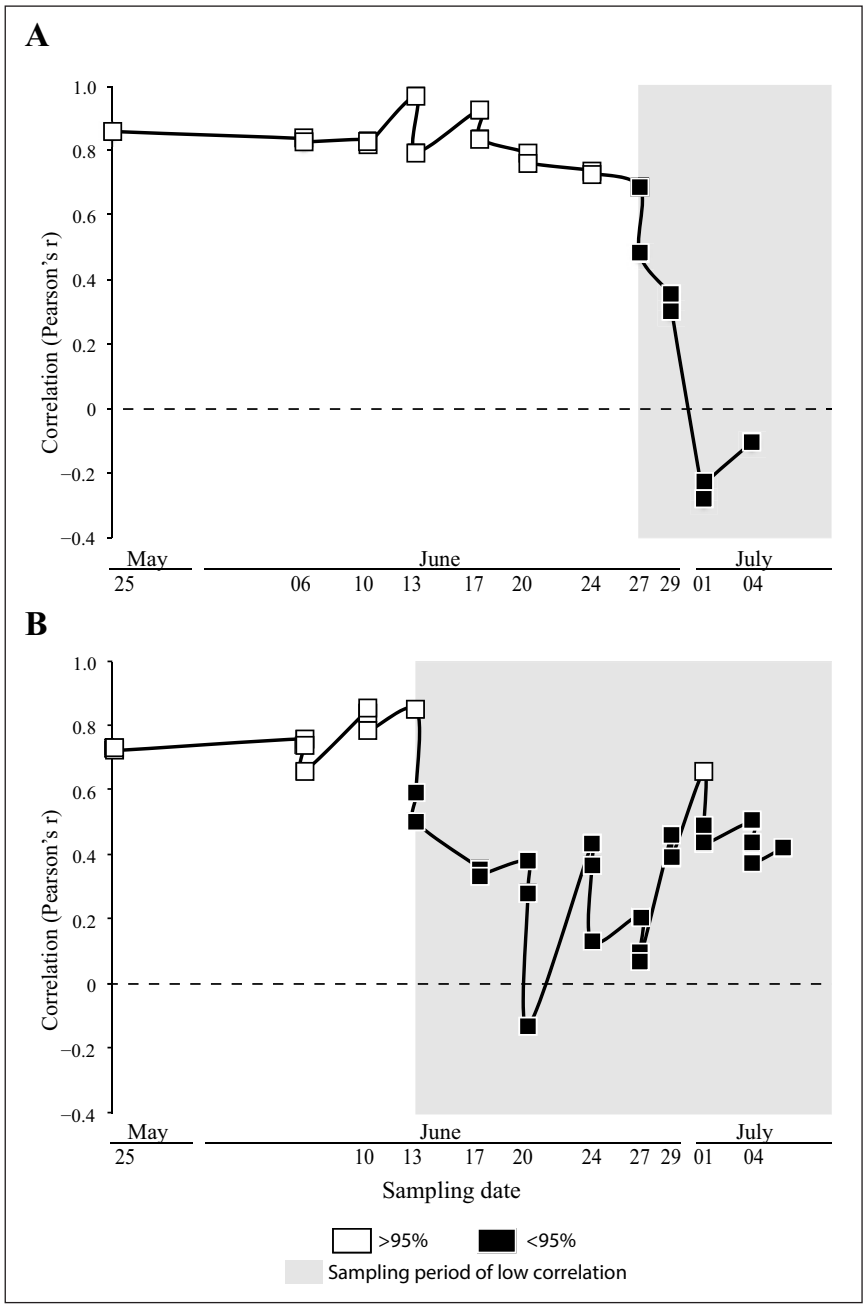

Figure 7: Correlation change-point analysis between the concentrations of Chl *a* and IP_{25}. Correlation change-point analysis between the concentrations of Chl *a* and IP_{25} collected in **(A)** near-surface (interface and 1.5 m) and **(B)** deeper water depths (10–40 m) from 18 May to 8 July 2016 at the sampling location in Baffin Bay (Figure 2). The sampling period of generally low correlation (<95%, black squares) is indicated by grey shading. DOI: https://doi.org/10.1525/elementa.377.f7

concentrations in the near-surface suspended POM, as described earlier. In general, sinking POM increased from 15 June until the end of the sampling period. As previously observed in sea ice, IP_{25} and HBI IIa in sinking particles were well correlated (r = 0.95). HBI III concentration in sinking POM ranged from 0 to 12.4 ng m^{-2} d^{-1} (mean ± SD = 1.3 ± 3.1 ng m^{-2} d^{-1}; n = 34) and from 0 to 8.7 ng m^{-2} d^{-1} (mean ± SD = 1.8 ± 2.6 ng m^{-2} d^{-1}; n = 34) at 2 and 25 m, respectively. HBI III was only observed at 4 and 8 sampling dates over the study period at 2 and 25 m, respectively. As with IP_{25}, HBI III was more abundant in the shallower trap compared to the deeper trap only on 6 June and 17 June (**Table 4**).

4. Discussion

4.1. Characteristics of the sea ice melting process

Sea ice at the beginning of sampling had relatively high snow cover and brine salinity, with relatively low Chl *a* concentration in the bottom ice sections, indicative of pre-bloom conditions (**Figure 3**). Two Chl *a* maxima on 1 June and 13 June were observed under different snow cover conditions during the period investigated. The first Chl *a* maximum coincided with a snowfall episode, suggesting the accumulation of pigments (relative to carbon biomass) by sympagic algae to enhance their light absorption efficiency (Johnsen and Sakshaug, 1993). In contrast, the subsequent decreases in snow, ice thickness and brine

salinity were accompanied by the second Chl *a* concentration peak (13 June; **Figure 3**), consistent with the usual spring ice bloom event, which terminated around 1 July, as shown by a return to near pre-bloom Chl *a* values (**Figure 3C**).

The profile of IP_{25} concentration broadly followed that of Chl *a*, as expected, although the correlation between them was slightly lower (r = 0.6; **Table 3**) than that reported in a previous time-series study (Belt et al., 2013), possibly due to different protist communities between the two studies. Indeed, because the IP_{25}-producing species are normally only present as minor components (typically 1–5%; Brown et al., 2014c), observing some de-coupling of IP_{25} from Chl *a*, the more representative measure of total photosynthetic biota, may not be surprising. Moreover, changes in the intracellular biosynthesis of IP_{25} in response to changing environmental conditions (e.g., light, salinity, temperature), such as during a melting period, are also likely (Limoges et al., 2018). On the other hand, the strong correlation between IP_{25} and HBI IIa is consistent with their common source (Belt and Müller, 2013; Brown et al., 2014a; Belt, 2018). More generally, the production of IP_{25} (and HBI IIa) throughout the spring bloom and prior to the onset of ice melt is consistent with previous findings from other regions of the Canadian Arctic (Brown et al., 2011; Belt et al., 2013) and NE Greenland (Limoges et al., 2018).

4.2. Distribution of IP_{25} in sea ice and the water column along the melt season

Brown et al. (2011) conducted the first study of the vertical distribution of IP_{25} in sea ice cores taken from the western Canadian Arctic along a spring time series. However, analyses were limited mainly to the early part of the time series (mid-March to mid-April) with a break in sampling late April–May, so the dataset was not continuous. In addition, sea ice cores were taken from different sampling locations within the Amundsen Gulf, consisted of both landfast and drift ice, and were analysed at higher vertical resolution (i.e., every cm) only on two dates. Nevertheless, this initial study revealed a substantially higher IP_{25} content in the bottom 5 cm of sea ice, at least in comparison with the 5–10 cm sections. Further, the higher vertical resolution data suggested that IP_{25} production occurred mainly in sea ice sections with >5% brine volume.

Our new data confirm the main findings of Brown et al. (2011), including the identification of IP_{25} in all ice cores exceeding the 5% brine volume threshold believed to be important for favourable diatom colonisation and growth (Mock et al., 2003; Golden et al., 2007). However, the continuous HVR sea ice sampling in the current study has enabled some further temporal variations in the vertical distribution of IP_{25} to be identified. Thus, between 18 May and 8 June, during which time hypersaline brines prevailed and brine volumes exceeded 5%, IP_{25} content was predominantly (>86%) in the 0–2 cm sections. From ca. 8 June to 27 June, highest IP_{25} concentrations were also found in the 0–2 cm sections, but the percentage in the upper layers (i.e., 2–10 cm; **Table 2**) increased as brine conditions in the sea ice, as a whole, switched to hyposaline (**Figure 3B**). Finally, from 27 June to the end of sampling, IP_{25} was largely absent, with only trace amounts detected in the 1–2 cm section on 1 July (**Table 2**). The salinity switch in the sea ice, probably driven by the downward percolation of melted snow (**Figure 3A**), likely produced a thin hyposaline water layer at the ice/water interface. As such hyposaline conditions are well known to significantly reduce ice algal growth and survival (Gosselin et al., 1986; Ralph et al., 2007), we suggest that this (presumed) hyposaline layer primarily impacted the ice algae within the bottom-most sections of the sea ice, enhancing their release into the water column and, as a consequence, resulting in an increase in the $\%IP_{25}$ content in the upper sea ice layers. In support of this scenario, the occurrence of relatively low sea ice Chl *a* and IP_{25} concentration in the bottom ice on 6 June contrasts with the somewhat high values in the near-surface waters, indicative of a pulsed release of ice algal POM (**Figures 3C, 4D** and **Table 1**), as seen in some previous studies (Tamelander et al., 2008; Rontani et al., 2016; Brown et al., 2016, 2017). A second (and larger) pulse of ice algae occurred on 24 June as evidenced from the highest IP_{25} concentration in the surface waters (**Table 1**). Otherwise, relatively consistent IP_{25} content in surface waters from 6 June until the end of sampling is indicative of a generally diffuse release of sea ice algal material (**Table 1**).

Exceptionally, because the higher $\%IP_{25}$ in the upper sections of the ice cores did not always coincide with a reduction in the amount of IP_{25} in the bottom sea ice (e.g., 13 and 17 June; **Table 2**), some additional factors may also be important. These may include processes such as the migration or development of ice algae in upper sea ice sections in response to changing light (due to snow deposition, photo-inhibition) or osmotic (hyposalinity) factors (Aumack et al., 2014; Olsen et al., 2017). The current study therefore provides further spatial evidence for the production of IP_{25} during the spring sympagic bloom and reinforces its use as a binary indicator of Arctic sea ice when detected in sediments (Belt, 2018, 2019).

The main interval of ice algal release from sea ice beginning on 6 June is also evident from the occurrence of IP_{25} in virtually all of the suspended POM samples, with highest concentrations in the near-surface layers and a generally decreasing concentration with depth. Further, the protist composition between sea ice and near-surface waters was also very similar during this interval, with a dominance of pennate diatoms (**Figure 5**). Along the sampling period, pulsed release of ice algal POM occurred twice, on 6 and 24 June, as discussed above. The production of extracellular polymeric substances (EPS) by ice algae facilitates their attachment to sea ice and also the formation of micro-aggregates of algal cells that can remain intact even after ice melt (Riebesell et al., 1991). The overall aggregation state of ice algae impacts their sedimentation rate and thus their residence time within the euphotic zone. Further, aggregated ice algae tend to be less active metabolically than their unaggregated counterparts (Riebesell et al., 1991; Rontani et al., 2016). As we propose that ice algae in the bottommost sections of sea ice in the current

study experienced osmotic stress from 6 June, which likely reduced their survival (Ralph et al., 2007), our additional observation of enhanced sinking POM from this date onwards at both sampling depths and especially at 25 m (**Table 1**) is not surprising. Interestingly, prior to hyposaline conditions (reducing algal survival and enhancing their release and sinking potential), ice biota would have experienced hypersaline conditions, thus reducing bacterial survival, growth and their re-mineralization potential (Amiraux et al., 2017). The pulsed release of ice biota resulting from hyposaline stress should therefore lead to the release of highly aggregated ice algal POM associated with a bacterial community shaped by the previous hypersaline conditions (Amiraux et al., 2017). Thus, we suggest that the sea ice POM released from 6 June possessed a strong burial potential, which may, in part, explain the widespread occurrence of IP_{25} in surface sediments across the Arctic (for an overview, see Belt, 2018).

4.3. Development of an under-ice phytoplankton bloom

Despite the well-known strong light attenuation properties of sea ice, evidence has been growing over the last decade or so for the occurrence of under-ice phytoplankton blooms in the Arctic (e.g., Gradinger, 1996; Ichinomiya et al., 2008; Mundy et al., 2009; Arrigo et al., 2012; Boetius et al., 2013; Assmy et al., 2017; Johnsen et al., 2018). Indeed, the assumption has been that some light availability is at least one of the determining factors controlling phytoplankton bloom occurrence, and Letelier et al. (2004) suggested a threshold value for PAR (0.415 E m^{-2} d^{-1}) in the subtropical North Pacific gyre, a value considered as a reference in the Arctic (Behrenfeld et al., 2017).

In the current study, this PAR threshold was first reached in the water column on 8 June, coinciding with substantially reduced snow cover (**Figure 3A**). With the exception of the relatively high near-surface Chl *a* values on 6 June and 24 June, likely due to the release of sea ice algae (see above), Chl *a* in suspended POM collected at all water depths was relatively low until 24 June (<1.2 µg L^{-1} up to 20 m depth). However, from 6 June the steady increase in under-ice PAR was accompanied by a clear increase in Chl *a*, especially after 24 June, suggesting either an under-ice phytoplankton bloom or an ice algae seeding event (**Figure 4C, D**). Significantly, the increase in Chl *a* was not accompanied by an increase in IP_{25} concentration (**Table 1**), which likely explains the poor correlation between Chl *a* and IP_{25} in SPM samples (r = 0.16), and the protist community on 8 July shifted from pennate to centric diatoms and phytoplankton (including *Chaetoceros* spp.) in sea ice and the water column, respectively (**Figure 5**). Interestingly, colonial centric *Chaetoceros* spp. have been reported to occur along the MIZ (e.g., Wassmann et al., 1999; Poulin et al., 2011) and often in highest concentration later in the season (e.g., Von Quillfeldt, 2000; Krawczyk et al., 2014). Thus, we attribute the increase in water column Chl *a* from 24 June to an under-ice phytoplankton bloom.

In order to investigate in more detail the point at which the composition of the SPM changed from predominantly ice algae to one that also included the under-ice phytoplankton bloom, we analysed the timing of significant correlation shifts between IP_{25} and Chl *a* in SPM collected at shallow (interface and 1.5 m) and deep (10, 20 and 40 m) samples (**Figure 7**). This analysis revealed that the significant change-point for shallow waters occurred later than for the deeper samples (27 June and 13 June, respectively), thus confirming, first, the stronger influence of ice algae at shallow water depths and, second, that the development of the main under-ice phytoplankton bloom from 24 June may have started earlier (13 June), coinciding with when the PAR threshold for such events was exceeded for most water depths (**Figure 4C**).

The identification of a temporal evolution of sea ice algal deposition and subsequent development of an under-ice phytoplankton bloom implies a variable contribution of sea ice POM to the underlying water column through the melt season. We therefore aimed to investigate whether this contribution could be expressed more quantitatively, especially as such determinations could have important implications for determining the relative contributions of OM from different sources more generally. In a recent study, Brown et al. (2016) proposed a method for calculating the percentage of ice-derived particulate organic carbon in seawater (%$iPOC_w$) based on the changes to the relative amounts of POC and IP_{25} in sea ice and the underlying water column. This approach also uses an end-member value for POC/IP_{25} in sea ice (i.e., $iPOC_i/IP_{25i}$), a feature identified as a possible limitation given its likely variability (Brown et al., 2016). Nevertheless, reasonable estimates for %$iPOC_w$ were obtained in the initial study by Brown et al. (2016), who also used the approach to provide evidence for an under-ice phytoplankton bloom. Brown et al. (2016) also suggested that the most reliable %$iPOC_w$ estimates were obtained using an $iPOC_i/IP_{25i}$ ratio measured during the interval of highest IP_{25} production. In the current study, the more frequent sampling arguably enabled this optimal $iPOC_i/IP_{25i}$ to be better identified. Consistent with the data of Brown et al. (2016), we observed $iPOC_i/IP_{25i}$ values during the interval of highest IP_{25i} concentration to be in the range from ca. 10^3 to 10^4. Moreover, we also obtained the most realistic estimates of %$iPOC_w$ using the $iPOC_i/IP_{25i}$ ratio obtained on 17 June, the sampling date of highest IP_{25} concentration in the 0–3 cm sea ice section.

Estimates of %$iPOC_w$ confirmed our previous findings based on Chl *a* and IP_{25} concentrations (**Figure 6**). For example, highest %$iPOC_w$ values were observed in surface waters collected on 6 June and 24 June, consistent with the proposed pulsed release of ice algal material. Further, a comparison between our %$iPOC_w$ estimates and the outcomes from the aforementioned change-point analysis of Chl *a* and IP_{25} concentrations provided additional information. Thus, during the early sampling period from 16 May to 6 June, the good correlation between IP_{25} and Chl *a* yet relatively low %$iPOC_w$ estimates for the deep SPM samples collected suggests only a minor contribution from both sympagic and pelagic algae to the total POC_w. In contrast, between 6 June and 13 June the relatively high %$iPOC_w$ estimates together with a still good correlation between IP_{25} and Chl *a* indicate the high contribution of sympagic algae to the total POM_w as they are released from the sea ice. Finally, from 13 June onwards, lower %$iPOC_w$ and a

poor correlation between Chl *a* and IP_{25} can be attributed to the initiation and then continuation of the under-ice bloom event (**Figures 6, 7**).

Identification of the optimal value for $iPOC_i/IP_{25i}$ remains problematic for all of the reasons described in detail by Brown et al. (2016). However, we note that in the current study, use of the lowest $iPOC_i/IP_{25i}$ value (obtained at highest IP_{25} concentration) resulted in only two samples exceeding 100% for $\%iPOC_w$ (i.e., the interface waters collected on 6 June and 24 June), and these were still within a factor of two of the theoretical limit. In any case, although we still suggest applying some caution to the absolute values for $\%iPOC_w$, the relative changes appear to provide realistic qualitative changes to the variable contribution of ice algal POC to a mixed pool, especially if these data are considered alongside other parameters, including taxonomy and change-point analysis, as described here.

4.4. Other HBIs in sea ice and the water column – possible implications for the PIP_{25} index

Of the previous investigations into HBIs in Arctic sea ice, all have focused mainly on the presence and quantification of IP_{25}, with much less attention given to other HBIs, including HBI IIa (Belt, 2018). Some earlier identification of other HBIs in sea ice have been reported, however, though these were mainly qualitative (Belt et al., 2007; Brown, 2011; Ringrose, 2012). Following the purification of standards, the development of improved analytical protocols (Belt et al., 2012), and the high sample volumes filtered in the current study, we were able to quantify other HBIs (i.e., HBIs IIa, IIb, III and IV) in some of our samples. As previously discussed, IP_{25} and HBI IIa co-occurred and were strongly correlated in all sample types (**Table 3**), consistent with common sources (Brown et al., 2014a, 2014b; Limoges et al., 2018). Similarly, HBIs IIb, III and IV were also strongly correlated in sea ice but much less so with IP_{25} and HBI IIa (**Table 3**) and, therefore, are assumed to have common sources, but different sources than those of IP_{25} and HBI IIa. Unfortunately, the concentrations of HBIs IIb, III and IV were mainly too low in the water column samples (e.g., **Table 4**) to permit satisfactory correlation analyses between them. HBIs III and IV have been reported previously in the benthic diatom *Pleurosigma intermedium* (Belt et al., 2000b) and in several planktonic diatoms belonging to the *Rhizosolenia* genus, (Rowland et al., 2001a; Belt et al., 2017), but thus far the co-occurrence of HBI IIb in such species has not been reported. However, neither *P. intermedium* nor *R. setigera* are ice-obligate species, so the identification of HBIs III and IV in sea ice has been attributed previously to the likely presence of certain phytoplankton entrapped within the sea ice matrix or brine channels (Brown et al., 2011; Rontani et al., 2014) rather than to production by strictly sympagic species. Interestingly, the co-production of HBIs IIb and IV has been reported in *Berkeleya rutilans*, a tube-dwelling diatom (Brown et al., 2014b) which, although belonging to a genus common in coastal and brackish environments from almost all latitudes (Round and Brooks, 1973; Cox, 1975; Lobban, 1984; Guiry and Guiry, 2013), has also been recorded within sea ice diatom communities from the Arctic (von Quillfeldt, 1997). In the study by Brown et al. (2014b), HBI III was not detected in the culture of *B. rutilans*, possibly due to too low abundance rather than strict absence, especially as HBI IV was only present as a minor constituent (ca. 7%; Brown et al., 2014b). Indeed, in our sea ice and water column samples, the average concentration of HBI III was 4.6 times lower than that of HBI IV, so may have simply been below detection limits in culture.

HBIs IIb, III and IV could be identified and quantified in almost all the LVR and HVR sea ice samples collected between the beginning of the sampling period and the first main occurrence of ice algal release (i.e., 16 May to 6 June). Thereafter, they were largely below detection limits (**Table 4**), suggesting a modification of the protist composition, with HBI III-producers possibly even more sensitive to hyposaline conditions than the sources of IP_{25} and HBI IIa. An increase in the ratio HBI III/IP_{25} between the 0–3 cm sea ice section and the underlying surface waters on 6 June (0.02 and 0.08, respectively) certainly supports the notion of a preferential release of producers of HBIs IIb, III and IV during the first algal release event. However, in the case of such producers still being present in the sea ice matrix after 6 June, the general failure to detect HBIs IIb, III and IV during an interval when IP_{25} was mainly quantifiable indicates either (i) their low contribution in the protist community (at least compared to before 6 June), (ii) a switching-off in their HBI production or (iii) their poor physiological state. Indeed, photodegradation processes (i.e., type II photosensitized processes) are dependent on both the residence time of phototrophic cells within the euphotic layer (Zafiriou et al., 1984; Mayer et al., 2009) and the extent of their senescence (Brown et al., 1989; Merzlyak and Hendry, 1994). Thus, as HBIs III and IV are known to be highly reactive toward such processes (Rontani et al., 2011, 2014), at least under laboratory conditions, the poor physiological state of producers of HBIs IIb, III and IV in sea ice could potentially result in their relatively rapid degradation. On the other hand, the quantification of the same HBIs within the water column following the 6 June ice algae release (**Table 4**) indicates that the higher sinking rate of such species can mitigate against such degradative removal. As such, the identification of HBIs IIb, III and IV in some Arctic sediments (Belt et al., 2008; Brown, 2011) may potentially result from release of some of their producers from sea ice.

The development of the so-called PIP_{25} index (phytoplankton marker-$IP_{25;}$ Müller et al., 2011) in recent years has provided, in some cases, more detailed descriptions of palaeo Arctic sea ice conditions than using IP_{25} alone (e.g., Fahl and Stein, 2012; Müller et al., 2012; Cabedo-Sanz et al., 2013; Stein and Fahl, 2013; Berben et al., 2014; Müller and Stein, 2014; Belt, 2018). The robustness of this index is dependant, in part, on the unequivocal source-specificity of the sympagic and pelagic biomarkers. Although IP_{25} appears to represent a suitable sympagic biomarker due to its source specificity (Brown et al., 2014c), identification of the most suitable pelagic counterpart remains challenging (Belt, 2018), especially as the commonly used sterol biomarkers such as epi-brassicasterol can have diverse sources (Huang and Meinschein, 1976; Volkman,

1986, 1998; Belt, 2018). In contrast, in some more recent studies, the use of some other HBIs (including HBI III) has been suggested as possibly better pelagic counterparts to IP_{25} owing to their apparently better source selectivity (i.e., certain marine diatoms). Indeed, some palaeo sea ice reconstructions based on PIP_{25} data derived from sedimentary IP_{25} and HBI III concentrations have appeared in recent years (see Belt, 2018), with semi-quantitative estimates of palaeo Arctic spring sea ice concentration in some cases (Smik et al., 2016b; Belt, 2018; Köseoğlu et al., 2018). However, data from the current study suggests that HBI III may not be as source-specific as originally believed, with some potential contribution from sea ice algae to the sedimentary budget. On the other hand, the isotopic composition of HBI III in the albeit relatively small number of measurements carried out thus far in the Arctic and Antarctic suggests that the majority (if not all) of the sedimentary contribution is derived from pelagic phytoplankton sources (e.g., Massé et al., 2001; Belt et al., 2008; Smik et al., 2016a; Belt, 2018). In further support of this suggestion, we note the substantially higher relative amount of HBI IV compared to HBI III in our sea ice and water column samples (mean enhancement of HBI IV is 4.6; see earlier), whereas the opposite is normally the case in Arctic and Antarctic sediments. Thus HBI III is normally ca. 3–4 times more abundant than HBI IV in sediments from the Barents Sea (Arctic) and around the Antarctic (Smik, 2016; Köseoğlu et al., 2018), and, importantly, this enhancement was also evident in several *Rhizosolenia* species isolated from mixed phytoplankton assemblages from both regions (Belt et al., 2017).

At this point, our new observations and interpretations are limited in two ways. First, we are unable to confirm the strict origin of HBIs IIb, III and IV in our sea ice and water column samples due to the absence of stable isotope ($\delta^{13}C$) data. Second, as studies of HBIs in sea ice are still relatively few in number (Belt, 2018), the extent to which the new findings are location-specific or representative of other Arctic regions is not clear. Both aspects need further attention before the broader significance of the new findings can be fully understood.

5. Conclusions

The sea ice proxy biomarker IP_{25} and other HBIs were identified and quantified in a time series of sea ice cores and in suspended and sinking particles sampled from the underlying water column across a single spring bloom and ice melt season in Baffin Bay (Canadian Arctic). The measurement of IP_{25} at high temporal and vertical resolution allowed us to highlight: (i) some production variability within sea ice, likely as a result of changes in brine salinity; (ii) the release of ice algae with high sinking rates following the switch of sea ice salinity from hypersaline to hyposaline conditions within the sampling period; and (iii) an under-ice phytoplankton bloom, as shown by a reduction in the contribution of sea ice organic carbon in the water column commensurate with a decoupling between IP_{25} concentration and Chl *a* concentrations. Other di- and tri-unsaturated HBIs were also quantified in some of the samples, with *Berkeleya rutilans* and/or species belonging to the *Pleurosigma* and *Rhizosolenia* genera suggested as potential sources. Although the strict origin of these HBIs remains uncertain at this stage, their occurrence in sea ice was restricted to early sampling dates, with their source(s) likely released to the water column during the first discharge of ice algae. Such HBIs may subsequently become deposited in underlying sediments, but the impact of this deposition on their use as possible pelagic counterparts to IP_{25} when using the PIP_{25} index requires further investigation. Our initial assessment of this aspect suggests that the contribution of such di- and tri-unsaturated HBIs to sediments from sea ice is much lower than from open water phytoplankton.

Data Accessibility Statement

All data are accessible at the Green Edge database (http://www.obs-vlfr.fr/proof/php/GREENEDGE/greenedge.php) and will be made public after publication.

Acknowledgements

This project would not have been possible without the support of the Hamlet of Qikiqtarjuaq and the members of the community as well as the Inuksuit School and its Principal Jacqueline Arsenault. The project is conducted under the scientific coordination of the Canada Excellence Research Chair in Remote Sensing of Canada's New Arctic frontier and the CNRS and Université Laval Takuvik Joint International laboratory (UMI3376). We thank Françoise Pinczon du Sel and Eric Brossier from Vagabond for assistance on the field and Yves Christen for fixing our valuable snowmobiles. The field campaign was successful thanks to the contributions of F. Bruyant, J. Larivière, E. Rehm, C. Aubry, C. Lalande, A. LeBaron, C. Marty, J. Sansoulet, D. Christiansen-Stowe, A. Wells, M. Benoît-Gagné, and E. Devred from the Takuvik laboratory, and C.J. Mundy from the University of Manitoba. We also thank Michel Gosselin, Québec-Océan, the CCGS *Amundsen* and the Polar Continental Shelf Program for their in-kind contribution in polar logistic and scientific equipment. We thank all participants in the Green Edge campaign for their contribution to the field work and data collection. We are grateful to the Editor, Jody Deming, and the two reviewers, Audrey Limoges and one anonymous, for providing helpful comments on a previous version of the manuscript.

Funding information

The Green Edge project is funded by the following French and Canadian programs and agencies: ANR (Contract #111112), CNES (project #131425), IPEV (project #1164), CSA, Fondation Total, ArcticNet, LEFE and the French Arctic Initiative (Green Edge project).

Competing interests

The authors have no competing interests to declare.

Author contributions

- R. Amiraux, J.-F. Rontani, M. Babin and S.T. Belt led the design of the study
- R. Amiraux led the writing, to which S.T. Belt contributed

- R. Amiraux led the analysis and made the figures with contributions from D. Köseoğlu and P.-L., Grondin
- R. Amiraux and V. Galindo led the sampling of brine, sea ice and snow thickness data
- R. Amiraux and L. Smik led the analysis of lipids
- All authors revised the earlier version of the manuscript, helped in the interpretation and approved the final version for publication

References

Amiraux, R, Belt, ST, Vaultier, F, Galindo, V, Gosselin, M, Bonin, P and **Rontani, J-F.** 2017. Monitoring photo-oxidative and salinity-induced bacterial stress in the Canadian Arctic using specific lipid tracers. *Mar Chem* **194**: 89–99. DOI: https://doi.org/10.1016/j.marchem.2017.05.006

Arrigo, KR, Perovich, DK, Pickart, RS, Brown, ZW, Van Dijken, GL, Lowry, KE, Mills, MM, Palmer, MA, Balch, WM and **Bahr, F.** 2012. Massive phytoplankton blooms under Arctic sea ice. *Science*: 1215065.

Assmy, P, Fernández-Méndez, M, Duarte, P, Meyer, A, Randelhoff, A, Mundy, CJ, Olsen, LM, Kauko, HM, Bailey, A and **Chierici, M.** 2017. Leads in Arctic pack ice enable early phytoplankton blooms below snow-covered sea ice. *Sci Rep-UK* **7**: 40850. DOI: https://doi.org/10.1038/srep40850

Aumack, C, Juhl, A and **Krembs, C.** 2014. Diatom vertical migration within land-fast Arctic sea ice. *J Marine Syst* **139**: 496–504. DOI: https://doi.org/10.1016/j.jmarsys.2014.08.013

Bates, SS and **Cota, GF.** 1986. Fluorescence induction and photosynthetic responses of Arctic ice algae to sample treatement and salinity. *J Phycol* **22**(4): 421–429. DOI: https://doi.org/10.1111/j.1529-8817.1986.tb02484.x

Behrenfeld, MJ, Hu, Y, O'Malley, RT, Boss, ES, Hostetler, CA, Siegel, DA, Sarmiento, JL, Schulien, J, Hair, JW and **Lu, X.** 2017. Annual boom–bust cycles of polar phytoplankton biomass revealed by space-based lidar. *Nat Geosci* **10**(2): 118. DOI: https://doi.org/10.1038/ngeo2861

Belt, ST. 2018. Source-specific biomarkers as proxies for Arctic and Antarctic sea ice. *Org Geochem* **125**: 277–298. DOI: https://doi.org/10.1016/j.orggeochem.2018.10.002

Belt, ST. 2019. What do IP_{25} and related biomarkers really reveal about sea ice change? *Quaternary Sci Rev* **204**: 216–219. DOI: https://doi.org/10.1016/j.quascirev.2018.11.025

Belt, ST, Allard, WG, Massé, G, Robert, J-M and **Rowland, SJ.** 2000a. Highly branched isoprenoids (HBIs): identification of the most common and abundant sedimentary isomers. *Geochim Cosmochim Acta* **64**(22): 3839–3851. DOI: https://doi.org/10.1016/S0016-7037(00)00464-6

Belt, ST, Allard, WG, Massé, G, Robert, J-M and **Rowland, SJ.** 2000b. Important sedimentary sesterterpenoids from the diatom. *Pleurosigma intermedium. Chem Commun*, 501–502. DOI: https://doi.org/10.1039/a909670a

Belt, ST, Allard, WG, Massé, G, Robert, J-M and **Rowland, SJ.** 2001. Structural characterisation of C_{30} highly branched isoprenoid alkenes (rhizenes) in the marine diatom *Rhizosolenia setigera. Tetrahedron Lett* **42**(32): 5583–5585. DOI: https://doi.org/10.1016/S0040-4039(01)01063-2

Belt, ST, Brown, TA, Navarro-Rodriguez, A, Cabedo-Sanz, P, Tonkin, A and **Ingle, R.** 2012. A reproducible method for the extraction, identification and quantification of the Arctic sea ice proxy IP_{25} from marine sediments. *Anal Methods-UK* **4**: 705–713. DOI: https://doi.org/10.1039/c2ay05728j

Belt, ST, Brown, TA, Ringrose, AE, Cabedo-Sanz, P, Mundy, CJ, Gosselin, M and **Poulin, M.** 2013. Quantitative measurement of the sea ice diatom biomarker IP_{25} and sterols in Arctic sea ice and underlying sediments: Further considerations for palaeo sea ice reconstrucion. *Org Geochem* **62**: 33–45. DOI: https://doi.org/10.1016/j.orggeochem.2013.07.002

Belt, ST, Brown, TA, Smik, L, Tatarek, A, Wiktor, J, Stowasser, G, Assmy, P, Allen, CS and **Husum, K.** 2017. Identification of C_{25} highly branched isoprenoid (HBI) alkenes in diatoms of the genus *Rhizosolenia* in polar and sub-polar marine phytoplankton. *Org Geochem* **110**: 65–72. DOI: https://doi.org/10.1016/j.orggeochem.2017.05.007

Belt, ST, Cabedo-Sanz, P, Smik, L, Navarro-Rodriguez, A, Berben, SMP, Knies, J and **Husum, K.** 2015. Identification of paleo Arctic winter sea ice limits and the marginal ice zone: Optimised biomarker-based reconstructions of late Quaternary Arctic sea ice. *Earth Planet Sci Lett* **431**: 127–139. DOI: https://doi.org/10.1016/j.epsl.2015.09.020

Belt, ST, Cooke, DA, Robert, J-M and **Rowland, S.** 1996. Structural characterisation of widespread polyunsaturated isoprenoid biomarkers: A C_{25} triene, tetraene and pentaene from the diatom *Haslea ostrearia* simonsen. *Tetrahedron Lett* **37**(27): 4755–4758. DOI: https://doi.org/10.1016/0040-4039(96)00926-4

Belt, ST, Massé, G, Rowland, SJ, Poulin, M, Michel, C and **LeBlanc, B.** 2007. A novel chemical fossil of palaeo sea ice: IP_{25}. *Org Geochem* **38**: 16–27. DOI: https://doi.org/10.1016/j.orggeochem.2006.09.013

Belt, ST, Massé, G, Vare, LL, Rowland, SJ, Poulin, M, Sicre, M-A, Sampei, M and **Fortier, L.** 2008. Distinctive ^{13}C isotopic signature distinguishes a novel sea ice biomarker in Arctic sediments and sediment traps. *Marine Chem* **112**(3–4): 158–167. DOI: https://doi.org/10.1016/j.marchem.2008.09.002

Belt, ST and **Müller, J.** 2013. The Arctic sea ice biomarker IP_{25}: a review of current understanding, recommendations for future research and applications in palaeo sea ice reconstructions. *Quaternary Sci Rev* **79**: 9–25. DOI: https://doi.org/10.1016/j.quascirev.2012.12.001

Belt, ST, Smik, L, Brown, TA, Kim, JH, Rowland, SJ, Allen, CS, Gal, JK, Shin, KH, Lee, JI and **Taylor,**

KWR. 2016. Source identification and distribution reveals the potential of the geochemical Antarctic sea ice proxy $IPSO_{25}$. *Nature Commun* **7**. DOI: https://doi.org/10.1038/ncomms12655

Belt, ST, Smik, L, Köseoğlu, D, Knies, J and **Husum, K.** 2019. A novel biomarker-based proxy for the spring phytoplankton bloom in Arctic and sub-arctic settings–HBI T_{25}. *Earth Planet Sci Lett* **523**: 115703. DOI: https://doi.org/10.1016/j.epsl.2019.06.038

Berben, S, Husum, K, Cabedo-Sanz, P and **Belt, S.** 2014. Holocene sub-centennial evolution of Atlantic water inflow and sea ice distribution in the western Barents Sea. *Clim Past* **10**(1): 181–198. DOI: https://doi.org/10.5194/cp-10-181-2014

Boetius, A, Albrecht, S, Bakker, K, Bienhold, C, Felden, J, Fernández-Méndez, M, Hendricks, S, Katlein, C, Lalande, C, Krumpen, T, Nicolaus, M, Peeken, I, Rabe, B, Rogacheva, A, Rybakova, E, Somavilla, R, Wenzhöfer, F and **the RV Polarstern ARK27-3-Shipboard Science Party.** 2013. Export of algal biomass from the melting Arctic sea ice. *Science* **339**(6126): 1430–1432. DOI: https://doi.org/10.1126/science.1231346

Brown, TA. 2011. Production and preservation of the Arctic sea ice diatom biomarker IP_{25} [PhD thesis]. Plymouth: University of Plymouth. Available at https://pearl.plymouth.ac.uk/bitstream/handle/10026.1/8169/2016smik10185302phd.pdf?sequence=1&isAllowed=n.

Brown, TA, Alexander, C, Yurkowski, D, Ferguson, S and **Belt, S.** 2014a. Identifying variable sea ice carbon contributions to the Arctic ecosystem: A case study using highly branched isoprenoid lipid biomarkers in Cumberland Sound ringed seals. *Limnol Oceanogr* **59**(5): 1581–1589. DOI: https://doi.org/10.4319/lo.2014.59.5.1581

Brown, TA, Assmy, P, Hop, H, Wold, A and **Belt, ST.** 2017. Transfer of ice algae carbon to ice-associated amphipods in the high-Arctic pack ice environment. *J Plankton Res* **39**(4): 664–674. DOI: https://doi.org/10.1093/plankt/fbx030

Brown, TA and **Belt, ST.** 2012. Closely linked sea ice–pelagic coupling in the Amundsen Gulf revealed by the sea ice diatom biomarker IP_{25}. *J Plankton Res* **34**: 647–654. DOI: https://doi.org/10.1093/plankt/fbs045

Brown, TA, Belt, ST and **Cabedo-Sanz, P.** 2014b. Identification of a novel di-unsaturated C_{25} highly branched isoprenoid in the marine tube-dwelling diatom *Berkeleya rutilans*. *Environ Chem Lett* **12**(3): 455–460. DOI: https://doi.org/10.1007/s10311-014-0472-4

Brown, TA, Belt, ST, Gosselin, M, Levasseur, M, Poulin, M and **Mundy, CJ.** 2016. Quantitative estimates of sinking sea ice particulate organic carbon based on the biomarker IP_{25}. *Mar Ecol Progr Ser* **546**: 17–29. DOI: https://doi.org/10.3354/meps11668

Brown, TA, Belt, ST, Philippe, B, Mundy, CJ, Massé, G, Poulin, M and **Gosselin, M.** 2011. Temporal and vertical variations of lipid biomarkers during a bottom ice diatom bloom in the Canadian Beaufort Sea: further evidence for the use of the IP_{25} biomarker as a proxy for spring Arctic sea ice. *Polar Biol* **34**(12): 1857–1868. DOI: https://doi.org/10.1007/s00300-010-0942-5

Brown, TA, Belt, ST, Tatarek, A and **Mundy, CJ.** 2014c. Source identification of the Arctic sea ice proxy IP_{25}. *Nature Commun* **5**. DOI: https://doi.org/10.1038/ncomms5197

Brown, TA, Galicia, MP, Thiemann, GW, Belt, ST, Yurkowski, DJ and **Dyck, MG.** 2018. High contributions of sea ice derived carbon in polar bear (*Ursus maritimus*) tissue. *PloS ONE* **13**(1): e0191631. DOI: https://doi.org/10.1371/journal.pone.0191631

Brown, TA, Nelson, DE, Mathewes, RW, Vogel, JS and **Southon, JR.** 1989. Radiocarbon dating of pollen by Accelerator Mass Spectrometry. *Quaternary Res* **32**: 205–212. DOI: https://doi.org/10.1016/0033-5894(89)90076-8

Cabedo-Sanz, P. 2013. Identification of variability in subarctic sea ice conditions during the Younger Dryas and Holocene [PhD Thesis]. Plymouth: University of Plymouth. Available at https://pearl.plymouth.ac.uk/bitstream/handle/10026.1/2858/2013Cabedo%20Sanz10251271%20phd.pdf?sequence=1&isAllowed=y.

Cabedo-Sanz, P, Belt, ST, Knies, J and **Husum, K.** 2013. Identification of contrasting seasonal sea ice conditions during the Younger Dryas. *Quaternary Sci Rev* **79**: 74–86. DOI: https://doi.org/10.1016/j.quascirev.2012.10.028

Cabrieto, J, Adolf, J, Tuerlinckx, F, Kuppens, P and **Ceulemans, E.** 2018. Detecting long-lived autodependency changes in a multivariate system via change point detection and regime switching models. *Sci Rep-UK* **8**(1): 15637. DOI: https://doi.org/10.1038/s41598-018-33819-8

Cabrieto, J, Tuerlinckx, F, Kuppens, P, Grassmann, M and **Ceulemans, E.** 2017. Detecting correlation changes in multivariate time series: A comparison of four non-parametric change point detection methods. *Behav Res Methods* **49**(3): 988–1005. DOI: https://doi.org/10.3758/s13428-016-0754-9

Collins, LG, Allen, CS, Pike, J, Hodgson, DA, Weckström, K and **Massé, G.** 2013. Evaluating highly branched isoprenoid (HBI) biomarkers as a novel Antarctic sea-ice proxy in deep ocean glacial age sediments. *Quaternary Sci Rev* **79**: 87–98. DOI: https://doi.org/10.1016/j.quascirev.2013.02.004

Cox, EJ. 1975. Further studies on the genus *Berkeleya* Grev. *Brit Phycol J* **10**(2): 205–217. DOI: https://doi.org/10.1080/00071617500650191

Cox, GF and **Weeks, WF.** 1983. Equations for determining the gas and brine volumes in sea-ice samples. *J Glaciol* **29**(102): 306–316. DOI: https://doi.org/10.1017/S0022143000008364

Fahl, K and **Stein, R.** 2012. Modern seasonal variability and deglacial/Holocene change of central Arctic Ocean sea-ice cover: New insights from biomarker proxy

records. *Earth Planet Sci Lett* **351–352**: 123–133. DOI: https://doi.org/10.1016/j.epsl.2012.07.009

Gardner, WD, Richardson, MJ, Carlson, CA, Hansell, D and **Mishonov, AV.** 2003. Determining true particulate organic carbon: bottles, pumps and methodologies. *Deep Sea Res Pt II* **50**(3–4): 655–674. DOI: https://doi.org/10.1016/S0967-0645(02)00589-1

Garrison, DL and **Buck, KR.** 1986. Organism losses during ice melting: A serious bias in sea ice community studies. *Polar Biol* **6**(4): 237–239. DOI: https://doi.org/10.1007/BF00443401

Golden, KM, Eicken, H, Heaton, AL, Miner, J, Pringle, DJ and **Zhu, J.** 2007. Thermal evolution of permeability and microstructure in sea ice. *Geophys Res Lett* **34**(16). DOI: https://doi.org/10.1029/2007GL030447

Gordon, DC. 1971. Distribution of particulate organic carbon and nitrogen at an oceanic station in the central Pacific. *Deep Sea Research and Oceanographic Abstracts* **18**(11): 1127–1134. DOI: https://doi.org/10.1016/0011-7471(71)90098-2

Gosselin, M, Legendre, L, Therriault, JC, Demers, S and **Rochet, M.** 1986. Physical control of the horizontal patchiness of sea ice microalgae. *Mar Ecol Progr Ser* **29**(3): 289–298. DOI: https://doi.org/10.3354/meps029289

Gradinger, R. 1996. Occurrence of an algal bloom under Arctic pack ice. *Mar Ecol Progr Ser* **131**: 301–305. DOI: https://doi.org/10.3354/meps131301

Grossi, V, Beker, B, Geenevasen, JAJ, Schouten, S, Raphel, D, Fontaine, M-F and **Sinninghe Damsté, JS.** 2004. C_{25} highly branched isoprenoid alkene from the marine benthic diatom *Pleurosigma strigosum*. *Phytochemistry* **65**: 3049–3055. DOI: https://doi.org/10.1016/j.phytochem.2004.09.002

Guiry, M and **Guiry, G.** 2013. AlgaeBase. Galway: worldwide electronic publication, National University of Ireland. Available at http://www.algaebase.org.

He, D, Simoneit, BRT, Xu, Y and **Jaffé, R.** 2016. Occurrence of unsaturated C_{25} highly branched isoprenoids (HBIs) in a freshwater wetland. *Org Geochem* **93**: 59–67. DOI: https://doi.org/10.1016/j.orggeochem.2016.01.006

Huang, W-Y and **Meinschein, WG.** 1976. Sterols as source indicators of organic materials in sediments. *Geochim Cosmochim Acta* **40**(3): 323–330. DOI: https://doi.org/10.1016/0016-7037(76)90210-6

Ichinomiya, M, Gomi, Y, Nakamachi, M, Honda, M, Fukuchi, M and **Taniguchi, A.** 2008. Temporal variations in the abundance and sinking flux of diatoms under fast ice in summer near Syowa Station, East Antarctica. *Polar Sci* **2**(1): 33–40. DOI: https://doi.org/10.1016/j.polar.2008.01.001

James, NA and **Matteson, DS.** 2015. Change points via probabilistically pruned objectives. *arXiv 1505.04302*.

Johns, L, Wraige, EJ, Belt, ST, Lewis, CA, Massé, G, Robert, JM and **Rowland, SJ.** 1999. Identification of a C_{25} highly branched isoprenoid (HBI) diene in Antarctic sediments, Antarctic sea-ice diatoms and cultured diatoms. *Org Geochem* **30**: 1471–1475. DOI: https://doi.org/10.1016/S0146-6380(99)00112-6

Johnsen, G, Norli, M, Moline, M, Robbins, I, von Quillfeldt, C, Sørensen, K, Cottier, F and **Berge, J.** 2018. The advective origin of an under-ice spring bloom in the Arctic Ocean using multiple observational platforms. *Polar Biol* **41**(6): 1197–1216. DOI: https://doi.org/10.1007/s00300-018-2278-5

Johnsen, G and **Sakshaug, E.** 1993. Bio-optical characteristics and photoadaptive responses in the toxic and bloom-forming dinoflagellates *Gyrodinium aureolum*, *Gymnodinium galatheanum*, and two strains of *Prorocentrum minimum*. *J Phycol* **29**(5): 627–642. DOI: https://doi.org/10.1111/j.0022-3646.1993.00627.x

Köseoğlu, D, Belt, ST, Smik, L, Yao, H, Panieri, G and **Knies, J.** 2018. Complementary biomarker-based methods for characterising Arctic sea ice conditions: A case study comparison between multivariate analysis and the PIP_{25} index. *Geochim Cosmochim Acta* **222**: 406–420. DOI: https://doi.org/10.1016/j.gca.2017.11.001

Krawczyk, DW, Witkowski, A, Waniek, JJ, Wroniecki, M and **Harff, J.** 2014. Description of diatoms from the Southwest to West Greenland coastal and open marine waters. *Polar Biol* **37**(11): 1589–1606. DOI: https://doi.org/10.1007/s00300-014-1546-2

Letelier, RM, Karl, DM, Abbott, MR and **Bidigare, RR.** 2004. Light driven seasonal patterns of chlorophyll and nitrate in the lower euphotic zone of the North Pacific Subtropical Gyre. *Limnol Oceanogr* **49**(2): 508–519. DOI: https://doi.org/10.4319/lo.2004.49.2.0508

Limoges, A, Massé, G, Weckström, K, Poulin, M, Ellegaard, M, Heikkilä, M, Geilfus, N-X, Sejr, MK, Rysgaard, S and **Ribeiro, S.** 2018. Spring succession and vertical export of diatoms and IP_{25} in a seasonally ice-covered high Arctic fjord. *Front Earth Sci* **6**(226). DOI: https://doi.org/10.3389/feart.2018.00226

Lobban, CS. 1984. Marine tube-dwelling diatoms of eastern Canada: descriptions, checklist, and illustrated key. *Can J Botany* **62**(4): 778–794. DOI: https://doi.org/10.1139/b84-114

Massé, G, Belt, ST, Crosta, X, Schmidt, S, Snape, I, Thomas, DN and **Rowland, SJ.** 2011. Highly branched isoprenoids as proxies for variable sea ice conditions in the Southern Ocean. *Antarct Sci* **23**: 487–498. DOI: https://doi.org/10.1017/S0954102011000381

Massé, G, Rincé, Y, Cox, EJ, Allard, G, Belt, ST and **Rowland, SJ.** 2001. *Haslea salstonica* sp. nov. and *Haslea pseudostrearia* sp. nov. (Bacillariophyta), two new epibenthic diatoms from the Kingsbridge estuary, United Kingdom. *CR Acad Sci III-Vie* **324**(7): 617–626. DOI: https://doi.org/10.1016/S0764-4469(01)01330-0

Mayer, LM, Schick, LL, Hardy, KR and **Estapa, ML.** 2009. Photodissolution and other photochemical changes upon irradiation of algal detritus. *Limnol Oceanogr*

54(5): 1688–1698. DOI: https://doi.org/10.4319/lo.2009.54.5.1688

Merzlyak, MN and **Hendry, G.** 1994. Free radical metabolism, pigment degradation and lipid peroxidation in leaves during senescence. *P Roy Soc Edinb B* **102**: 459–471. DOI: https://doi.org/10.1017/S0269727000014482

Mock, T, Kruse, M and **Dieckmann, GS.** 2003. A new microcosm to investigate oxygen dynamics at the sea ice water interface. *Aquat Microb Ecol* **30**(2): 197–205. DOI: https://doi.org/10.3354/ame030197

Müller, J and **Stein, R.** 2014. High-resolution record of late glacial and deglacial sea ice changes in Fram Strait corroborates ice–ocean interactions during abrupt climate shifts. *Earth Planet Sci Lett* **403**: 446–455. DOI: https://doi.org/10.1016/j.epsl.2014.07.016

Müller, J, Wagner, A, Fahl, K, Stein, R, Prange, M and **Lohmann, G.** 2011. Towards quantitative sea ice reconstructions in the northern North Atlantic: A combined biomarker and numerical modelling approach. *Earth Planet Sci Lett* **306**(3–4): 137–148. DOI: https://doi.org/10.1016/j.epsl.2011.04.011

Müller, J, Werner, K, Stein, R, Fahl, K, Moros, M and **Jansen, E.** 2012. Holocene cooling culminates in sea ice oscillations in Fram Strait. *Quaternary Sci Rev* **47**(0): 1–14. DOI: https://doi.org/10.1016/j.quascirev.2012.04.024

Mundy, CJ, Gosselin, M, Ehn, J, Gratton, Y, Rossnagel, A, Barber, DG, Martin, J, Tremblay, J-E, Palmer, M, Arrigo, KR, Darnis, G, Fortier, L, Else, B and **Papakyriakou, T.** 2009. Contribution of under-ice primary production to an ice-edge upwelling phytoplankton bloom in the Canadian Beaufort Sea. *Geophys Res Lett* **36**. DOI: https://doi.org/10.1029/2009GL038837

Olsen, LM, Laney, SR, Duarte, P, Kauko, HM, Fernández-Méndez, M, Mundy, CJ, Rösel, A, Meyer, A, Itkin, P and **Cohen, L.** 2017. The seeding of ice algal blooms in Arctic pack ice: the multiyear ice seed repository hypothesis. *J Geophys Res-Biogeo* **122**(7): 1529–1548. DOI: https://doi.org/10.1002/2016JG003668

Oziel, L, Massicotte, P, Randelhoff, A, Ferland, J, Vladoiu, A, Lacour, L, Lambert-Girard, S, Dumont, D, Cuypers, Y, Bouruet-Aubertot, P, Galindo, V, Marec, C, Forget, M-H, Garcia, N, Raimbault, P, Houssais, M-N and **Babin, M.** 2019. Environmental factors influencing the seasonal dynamics of under-ice spring blooms in Baffin Bay. *Elem Sci Anth* (in press). DOI: https://doi.org/10.1525/elementa.372

Parsons, T, Maita, Y and **Lalli, C.** 1984. *A manual of chemical and biological methods for seawater analysis*. Totronto: Pergamon Press.

Picheral, M, Colin, S and **Irisson, J-O.** 2015. EcoTaxa, a tool for the taxonomic classification of images. Available at http://ecotaxa.obs-vlfr.fr.

Poulin, M, Daugbjerg, N, Gradinger, R, Ilyash, L, Ratkova, T and **von Quillfeldt, C.** 2011. The pan-Arctic biodiversity of marine pelagic and sea-ice unicellular eukaryotes: a first-attempt assessment. *Mar Biodivers* **41**(1): 13–28. DOI: https://doi.org/10.1007/s12526-010-0058-8

Ralph, PJ, Ryan, KG, Martin, A and **Fenton, G.** 2007. Melting out of sea ice causes greater photosynthetic stress in algae than freezing in 1. *J Phycol* **43**(5): 948–956. DOI: https://doi.org/10.1111/j.1529-8817.2007.00382.x

Riebesell, U, Schloss, I and **Smetacek, V.** 1991. Aggregation of algae released from melting sea ice – Implications for seeding and sedimentation. *Polar Biol* **11**(4): 239–248. DOI: https://doi.org/10.1007/BF00238457

Ringrose, AE. 2012. Temporal and vertical distributions of IP_{25} and other lipid biomarkers in sea ice from Resolute Bay, Nunavut, Canada. [MS thesis], University of Plymouth. Available at http://hdl.handle.net/10026.1/2880.

Robson, J and **Rowland, S.** 1986. Identification of novel widely distributed sedimentary acyclic sesterterpenoids. *Nature* **324**: 561–563. DOI: https://doi.org/10.1038/324561a0

Rontani, J-F, Belt, ST, Brown, TA, Amiraux, R, Gosselin, M, Vaultier, F and **Mundy, CJ.** 2016. Monitoring abiotic degradation in sinking versus suspended Arctic sea ice algae during a spring ice melt using specific lipid oxidation tracers. *Org Geochem* **98**: 82–97. DOI: https://doi.org/10.1016/j.orggeochem.2016.05.016

Rontani, J-F, Belt, ST, Vaultier, F and **Brown, TA.** 2011. Visible light induced photo-oxidation of highly branched isoprenoid (HBI) alkenes: Significant dependence on the number and nature of double bonds. *Org Geochem* **42**(7): 812–822. DOI: https://doi.org/10.1016/j.orggeochem.2011.04.013

Rontani, JF, Belt, ST, Vaultier, F, Brown, TA and **Massé, G.** 2014. Autoxidative and Photooxidative Reactivity of Highly Branched Isoprenoid (HBI) Alkenes. *Lipids* **49**(5): 481–494. DOI: https://doi.org/10.1007/s11745-014-3891-x

Round, F and **Brooks, M.** 1973. A new species of *Amphipleura* from Togo, W. Africa. *Bot Mar* **16**(2): 77–79. DOI: https://doi.org/10.1515/botm.1973.16.2.77

Rowland, SJ, Allard, W, Belt, S, Massé, G, Robert, J-M, Blackburn, S, Frampton, D, Revill, A and **Volkman, J.** 2001a. Factors influencing the distributions of polyunsaturated terpenoids in the diatom, *Rhizosolenia setigera*. *Phytochemistry* **58**(5): 717–728. DOI: https://doi.org/10.1016/S0031-9422(01)00318-1

Rowland, SJ, Belt, ST, Wraige, EJ, Massé, G, Roussakis, C and **Robert, JM.** 2001b. Effects of temperature on polyunsaturation in cytostatic lipids of *Haslea ostrearia*. *Phytochemistry* **56**(6): 597–602. DOI: https://doi.org/10.1016/S0031-9422(00)00434-9

Rowland, SJ and **Robson, JN.** 1990. The widespread occurrence of highly branched acyclic C_{20}, C_{25} and C_{30} hydrocarbons in recent sediments and biota–A review. *Mar Environ Res* **30**(3): 191–216. DOI: https://doi.org/10.1016/0141-1136(90)90019-K

Schlitzer, R. 2016. Ocean Data View, version 4.7.8.

Sinninghe-Damsté, JS, Muyzer, G, Abbas, B, Rampen, SW, Massé, G, Allard, WG, Belt, ST, Robert, JM, Rowland, SJ, Moldowan, JM, Barbanti, SM, Fago, FJ, Denisevich, P, Dahl, J, Trindade, LAF and **Schouten, S.** 2004. The rise of the rhizosolenid diatoms. *Science* **304**: 584–587. DOI: https://doi.org/10.1126/science.1096806

Sinninghe-Damsté, JS, Schouten, S, Rijpstra, WIC, Hopmans, EC, Peletier, H, Gieskes, WWC and **Geenevasen, JAJ.** 1999. Structural identification of the C_{25} highly branched isoprenoid pentaene in the marine diatom *Rhizosolenia setigera*. *Org Geochem* **30**(12): 1581–1583. DOI: https://doi.org/10.1016/S0146-6380(99)00140-0

Smik, L. 2016. Development of biomarker-based proxies for paleo sea-ice reconstructions. [PhD thesis] Plymouth: University of Plymouth. Available at https://pearl.plymouth.ac.uk/bitstream/handle/10026.1/8169/2016smik10185302phd.pdf?sequence=1&isAllowed=y.

Smik, L, Belt, ST, Lieser, JL, Armand, LK and **Leventer, A.** 2016a. Distributions of highly branched isoprenoid alkenes and other algal lipids in surface waters from East Antarctica: Further insights for biomarker-based paleo sea-ice reconstruction. *Org Geochem* **95**: 71–80. DOI: https://doi.org/10.1016/j.orggeochem.2016.02.011

Smik, L, Cabedo-Sanz, P and **Belt, ST.** 2016b. Semi-quantitative estimates of paleo Arctic sea ice concentration based on source-specific highly branched isoprenoid alkenes: A further development of the PIP_{25} index. *Org Geochem* **92**: 63–69. DOI: https://doi.org/10.1016/j.orggeochem.2015.12.007

Smith, SD, Muench, RD and **Pease, CH.** 1990. Polynyas and leads: An overview of physical processes and environment. *J Geophys Res-Oceans* **95**(C6): 9461–9479. DOI: https://doi.org/10.1029/JC095iC06p09461

Sosik, HM and **Olson, RJ.** 2007. Automated taxonomic classification of phytoplankton sampled with imaging-in-flow cytometry. *Limnol Oceanogr-Meth* **5**(6): 204–216. DOI: https://doi.org/10.4319/lom.2007.5.204

Stein, R and **Fahl, K.** 2013. Biomarker proxy shows potential for studying the entire Quaternary Arctic sea ice history. *Org Geochem* **55**: 98–102. DOI: https://doi.org/10.1016/j.orggeochem.2012.11.005

Tamelander, T, Reigstad, M, Hop, H, Carroll, ML and **Wassmann, P.** 2008. Pelagic and sympagic contribution of organic matter to zooplankton and vertical export in the Barents Sea marginal ice zone. *Deep Sea Res Pt II* **55**(20–21): 2330–2339. DOI: https://doi.org/10.1016/j.dsr2.2008.05.019

Volkman, JK. 1986. A review of sterol markers for marine and terrigenous organic matter. *Org Geochem* **9**(2): 83–99. DOI: https://doi.org/10.1016/0146-6380(86)90089-6

Volkman, JK, Barrett, SM, Blackburn, SI, Mansour, MP, Sikes, EI and **Gelin, F.** 1998. Microalgal biomarkers: A review of recent research developments. *Org Geochem* **29**(5–7): 1163–1179. DOI: https://doi.org/10.1016/S0146-6380(98)00062-X

Volkman, JK, Barrett, SM and **Dunstan, GA.** 1994. C_{25} and C_{30} highly branched isoprenoid alkenes in laboratory cultures of two marine diatoms. *Org Geochem* **21**: 407–414. DOI: https://doi.org/10.1016/0146-6380(94)90202-X

von Quillfeldt, CH. 1997. Distribution of diatoms in the Northeast Water Polynya, Greenland. *J Mar Systems* **10**(1–4): 211–240. DOI: https://doi.org/10.1016/S0924-7963(96)00056-5

von Quillfeldt, CH. 2000. Common diatom species in Arctic spring blooms: their distribution and abundance. *Bot Mar* **43**(6): 499–516. DOI: https://doi.org/10.1515/BOT.2000.050

Wassmann, P, Ratkova, T, Andreassen, I, Vernet, M, Pedersen, G and **Rey, F.** 1999. Spring bloom development in the marginal ice zone and the central Barents Sea. *Mar Ecol* **20**: 321–346. DOI: https://doi.org/10.1046/j.1439-0485.1999.2034081.x

Wraige, EJ, Belt, ST, Lewis, CA, Cooke, DA, Robert, JM, Massé, G and **Rowland, SJ.** 1997. Variations in structures and distributions of C_{25} highly branched isoprenoid (HBI) alkenes in cultures of the diatom, *Haslea ostrearia* (Simonsen). *Org Geochem* **27**: 497–505. DOI: https://doi.org/10.1016/S0146-6380(97)00086-7

Xu, Y, Jaffé, R, Wachnicka, A, Gaiser, EE. 2006. Occurrence of C_{25} highly branched isoprenoids (HBIs) in Florida Bay: Paleoenvironmental indicators of diatom-derived organic matter inputs. *Org Geochem* **37**(7): 847–859. DOI: https://doi.org/10.1016/j.orggeochem.2006.02.001

Zafiriou, OC, Joussot-Dubien, J, Zepp, RG and **Zika, RG.** 1984. Photochemistry of natural waters. *Environ Sci Technol* **18**(12): 358A–371A. DOI: https://doi.org/10.1021/es00130a711

How to cite this article: Amiraux, R, Smik, L, Köseoğlu, D, Rontani, J-F, Galindo, V, Grondin, P-L, Babin, M and Belt, ST. 2019. Temporal evolution of IP_{25} and other highly branched isoprenoid lipids in sea ice and the underlying water column during an Arctic melting season. *Elem Sci Anth,* 7: 38. DOI: https://doi.org/10.1525/elementa.377

Domain Editor-in-Chief: Jody W. Deming, School of Oceanography, University of Washington, US

Associate Editor: Kevin Arrigo, Environmental Earth System Science, Stanford University, US

Knowledge Domain: Ocean Science

Part of an *Elementa* Special Feature: Green Edge

Submitted: 07 June 2019 **Accepted:** 16 September 2019 **Published:** 01 October 2019

ELEMENTA Science of the Anthropocene

Elem Sci Anth is a peer-reviewed open access journal published by University of California Press.

OPEN ACCESS